July 2020

IEA Wind TCP Task 37

Definition of the UMaine VolturnUS-S Reference Platform Developed for the IEA Wind 15-Megawatt Offshore Reference Wind Turbine

Technical Report

iea wind

Definition of the UMaine VolturnUS-S Reference Platform Developed for the IEA Wind 15-Megawatt Offshore Reference Wind Turbine

Christopher Allen,[1] Anthony Viselli,[1] Habib Dagher,[1] Andrew Goupee,[1] Evan Gaertner,[2] Nikhar Abbas,[2] Matthew Hall,[2] and Garrett Barter[2]

1 University of Maine
2 National Renewable Energy Laboratory

Suggested Citation
Allen, Christopher, Anthony Viselli, Habib Dagher, Andrew Goupee, Evan Gaertner, Nikhar Abbas, Matthew Hall, and Garrett Barter. *Definition of the UMaine VolturnUS-S Reference Platform Developed for the IEA Wind 15-Megawatt Offshore Reference Wind Turbine*. Golden, CO: National Renewable Energy Laboratory. NREL/TP-5000-76773. https://www.nrel.gov/docs/fy20osti/76773.pdf.

NREL is a national laboratory of the U.S. Department of Energy
Office of Energy Efficiency & Renewable Energy
Operated by the Alliance for Sustainable Energy, LLC

This report is available at no cost from the National Renewable Energy Laboratory (NREL) at www.nrel.gov/publications.

Contract No. DE-AC36-08GO28308

Technical Report
NREL/TP-5000-76773
July 2020

National Renewable Energy Laboratory
15013 Denver West Parkway
Golden, CO 80401
303-275-3000 • www.nrel.gov

NOTICE

This work was authored [in part] by the National Renewable Energy Laboratory, operated by Alliance for Sustainable Energy, LLC, for the U.S. Department of Energy (DOE) under Contract No. DE-AC36-08GO28308. Funding provided by the U.S. Department of Energy Office of Energy Efficiency and Renewable Energy Wind Energy Technologies Office. The views expressed herein do not necessarily represent the views of the DOE or the U.S. Government.

Cover Photos by Dennis Schroeder: (clockwise, left to right) NREL 51934, NREL 45897, NREL 42160, NREL 45891, NREL 48097, NREL 46526.

List of Acronyms

DLC	design load case
DOF	degree of freedom
IEC	International Electrotechnical Commission
QTF	quadratic transfer function
RAO	response amplitude operator
RNA	rotor nacelle assembly
ROSCO	Reference OpenSource Controller
SWL	still water line
NREL	National Renewable Energy Laboratory
UMaine	University of Maine

Executive Summary

Reference wind turbines are an important component to the wind energy sector. They serve as publicly available benchmarks that can be openly used to explore new technologies and designs as well as aid in facilitating collaborative efforts between researchers and industry. Earlier this year, the International Energy Agency (IEA) 15-megawatt (MW) reference wind turbine was released and currently represents the largest publicly available reference machine (Gaertner et al. 2020). The size of the IEA 15-MW reference turbine mirrors the wind industry's trend of offshore machines with larger power ratings. According to the U.S. Department of Energy's "2018 Offshore Wind Technologies Market Report" and the American Wind Energy Association, significant development has occurred in the past few years that highlights the opportunity for targeted research investment in offshore wind (Musial et al. 2019). Several states including Massachusetts, New York, and Maryland have enacted new policies or bolstered their existing policies to support the development of over 4,000 MW of offshore wind energy. Looking to the near future, the U.S. offshore wind project development pipeline includes 25,824 MW of potential installed capacity (Musial et al. 2019).

Though the total U.S. offshore wind energy potential is more than twice what the entire country currently uses, nearly 60% of the U.S .offshore wind resource is located in deep water, requiring floating foundation technologies (Schwartz et al. 2010). In most commercial wind farms in Europe, and more recently the United States, offshore wind turbines are supported on monopoles in water depths up to 30 meters (m) and steel jacket structures from 25 m to about 50 m. In water depths over 50 m, where a majority of the U.S. offshore wind power potential lies, the cost of jacket foundations becomes prohibitively expensive, requiring the use of floating offshore wind turbine technologies.

This report serves as an addendum to *"*IEA Wind TCP Task 37: Definition of the IEA Wind 15-Megawatt Offshore Reference Wind Turbine" (Gaertner et al. 2020) and defines the University of Maine (UMaine) VolturnUS-S reference floating offshore wind turbine semisubmersible, designed to support the IEA 15-MW reference wind turbine. The design and arrangement described in this report are intended to generically represent future floating offshore wind turbine technology. In addition to the floating platform, this report also details the other floating-specific components of the floating offshore wind turbine including the mooring system, tower, and turbine controller.

Table of Contents

1 Introduction 1
2 Design Details 6
2.1 UMaine VolturnUS-S Semisubmersible Platform 6
2.2 Mooring System Properties 13
2.3 Floating Tower 15
2.4 Wind Turbine Controller 19
3 System Identification 20
3.1 Static Surge-Sway Offsets 20
3.2 Rigid-Body Free Decays 21
3.3 Response Amplitude Operators 23
4 System Performance Assessment 26
References 33

List of Figures

Figure 1. The UMaine VolturnUS-S reference platform designed to support the IEA-15-240 RWT system definition. *Figure courtesy of the University of Maine* 2
Figure 2. FOWT Reference coordinate system. *Figure courtesy of the University of Maine* 4
Figure 3. General arrangement. *Figure courtesy of the University of Maine* 5
Figure 4. Added mass and radiation damping vs. frequency evaluated by WAMIT 8
Figure 5. Radiation impulse-response functions 9
Figure 6. First-order wave excitation coefficients evaluated by WAMIT for a 0˚ wave heading 10
Figure 7. Difference (left) and sum (right) second-order wave forces for a wave heading of 0˚ evaluated by WAMIT 11
Figure 8. Surge steady-state flow (i.e., flow right to left) drag simulation in OpenFOAM showing the fluid's x-velocity in m/s 12
Figure 9. Mooring system arrangement within the inertia frame shown in plan (top) and elevation (bottom) views. *Figure courtesy of the University of Maine* 15
Figure 10. Tower natural frequencies relative to excitation frequencies 16
Figure 11. Tower structural properties vs. tower height above SWL 18
Figure 12. Fairlead and anchor tension vs. surge-sway offset 20
Figure 13. SWL surge and sway free-decay time histories (top) and damping ratio vs. initial cycle amplitude (bottom) 21
Figure 14. SWL heave free-decay time histories (top) and damping ratio vs. initial cycle amplitude (bottom) 22
Figure 15. SWL pitch and roll free-decay time histories (top) and damping ratio vs. initial cycle amplitude (bottom) 22
Figure 16. SWL yaw free-decay time histories (top) and damping ratio vs. initial cycle amplitude (bottom) 23
Figure 17. SWL surge RAO magnitude (top) and phase (bottom) 24
Figure 18. SWL heave RAO magnitude (top) and phase (bottom) 24
Figure 19. SWL pitch RAO magnitude (top) and phase (bottom) 25
Figure 20. RNA fore-aft RAO magnitude (top) and phase (bottom) 25
Figure 21. DLC acceleration statistics (m/s^2) 29
Figure 22. DLC deflection and displacement statistics (m or ˚) 30
Figure 23. DLC moment statistics (kN-m) 31
Figure 24. DLC force statistics (N) 32

List of Tables

Table 1. Floating Offshore Wind Turbine General System Properties 3
Table 2. Semisubmersible Platform Properties 6
Table 3. Hull Hydrostatic Stiffness Evaluated by WAMIT (N/m, N/rad or N-m/rad) 7
Table 4. Hull Infinite-Frequency Added Mass Evaluated by WAMIT (kg, kg-m or kg-m^2) 9
Table 5. Viscous Damping Matrix (N-s^2/m^2, N-s^2, N-s^2/m, N-m-s^2) 12
Table 6. Mooring System Properties 13
Table 7. Mooring Line Drag and Added Mass Coefficients 13
Table 8. Floating Tower Properties 17
Table 9. Steel Material Properties for the Floating Tower 17
Table 10. Tower Dimensions as a Function of Height 17
Table 11. Rigid-Body Natural Frequencies 21
Table 12. IEC Design Load Case Matrix 27
Table 13. OpenFAST Output Definitions 28

1 Introduction

This report defines the University of Maine (UMaine) VolturnUS-S reference floating offshore wind turbine semisubmersible designed to support the International Energy Agency (IEA)-15-240-RWT 15-megawatt (MW) reference wind turbine. The semisubmersible is a generic steel version of the UMaine patented concrete floating foundation technology developed in collaboration with the U.S. Department of Energy (Viselli et al. 2015a, 2015b; Viselli et al. 2014). This report serves as an addendum to "IEA Wind TCP Task 37: Definition of the IEA Wind 15-Megawatt Offshore Reference Wind Turbine" (Gaertner et al. 2020) and provides details on a floating semisubmersible design developed to support the 15-MW reference wind turbine.

The offshore wind turbine industry has rapidly increased the scale of its power capacity in recent years, with units between 8 and 12 MW now becoming the norm. As turbine size increases, the various other components associated with a floating offshore wind turbine system must evolve to accommodate the new design requirements of larger machines. The floating support system presented in this work has taken into consideration the current technological trends and is intended to generically represent future floating offshore wind turbine technology. This reference design was developed by UMaine and aims to serve the wind industry by providing a publicly available design benchmark to explore new technologies and design methodologies while facilitating collaboration between industry and researchers.

Depicted in Figure 1, the reference floating offshore wind turbine defined in this work comprises a floating semisubmersible platform, a chain catenary mooring system, a floating-specific tower, and a modified float-specific controller tuning that have been tailored specifically to the IEA-15-240-RWT defined by Gaertner et al. (2020). This reference floating offshore wind turbine system is intended to be distributed with the IEA-15-240-RWT to the wind energy community through the details specified in this report as well as open OpenFAST and HAWC2 models through the Github repository, located here: https://github.com/IEAWindTask37/IEA-15-240-RWT.

This report provides the data and system properties required for modeling the IEA-15-240-RWT floating offshore wind turbine. Section 2 provides a system overview that details the floating offshore wind turbine's arrangement and key system properties. Additionally, we provide the global coordinate system, which defines the floating offshore wind turbine within the inertia frame of the OpenFAST model. Following this are subsections that provide details of the individual subsystems of the floating offshore wind turbine, namely the floating platform, mooring system, turbine tower, and turbine controller. Section 3 includes results of system identification simulations, which include static offsets, rigid body free decays, and response amplitude operators of the system subjected to wave loading. Section 4 concludes with an assessment of the floating offshore wind turbine's performance under International Electrotechnical Commission (IEC) load cases selected to gauge performance in both normal and extreme conditions.

Figure 1. The UMaine VolturnUS-S reference platform designed to support the IEA-15-240 RWT system definition. ***Figure courtesy of the University of Maine***

The following section details the properties and arrangements of the UMaine VolturnUS-S semisubmersible reference floating offshore wind turbine and its various components that are shown in plan and elevation views in Figure 3 with general system properties provided in Table 1. Unless stated otherwise, all values reported in this work are with respect to the coordinate system defined in Figure 2. The system, which was designed to support the IEA-15-240-RWT, comprises a four-column, three-radial and one central, steel semisubmersible platform held on

station via a three-line catenary mooring array that is deployed in 200 meters (m) of water. The tower, which has been designed for this floating-specific application and differs from the tower released with the original monopile foundation (Gaertner et al. 2020), is connected to the central column of the platform and places the rotor nacelle assembly (RNA) at a hub height of 150 m above the still water line (SWL).

When installed, the platform has a draft of 20 m with a 15-m freeboard to the upper deck of the columns. The completely assembled unit displaces 20,206 cubic meters (m^3) of seawater (with an assumed density of 1,025 kilograms per cubic meter [kg/m^3]), which consists of a 1,263-t (metric tonne) tower, a 991-t RNA, and a 17,839-t ballasted platform with 6,065 kilonewtons (kN) of mooring vertical pretension. The system has an assumed deployment depth of 200 m and is held on to the station by a three-line chain catenary mooring system. The lines of the spread catenary system span radially to anchors located 837.60 m from the tower's centerline.

Note that properties and specifications of the IEA-15-240-RWT turbine can be found in the previously published report, "IEA Wind TCP Task 37: Definition of the IEA Wind 15-Megawatt Offshore Reference Wind Turbine" (Gaertner et al. 2020) and, as such, are not provided here.

Table 1. Floating Offshore Wind Turbine General System Properties

Parameter	Units	Value
Turbine Rating	MW	15
Hub Height	m	150
Excursion[1] (Length, Width, Height)	m	90.1, 102.1, 290.0
Platform Type		semisubmersible
Freeboard	m	15
Draft	m	20
Total System Mass	t	20,093
Platform Mass	t	17,839
Tower Mass	t	1,263
RNA Mass	t	991
Water Depth	m	200
Mooring System	-	Three-line chain catenary

[1] The system's excursion describes the volume encompassed by the complete structure. In Figure 3, the length and width define the distance of the system's outermost points along the x-axis and y-axis, respectively. Similarly, the height defines the total distance from the keel to the top of the rotor diameter along the z-axis.

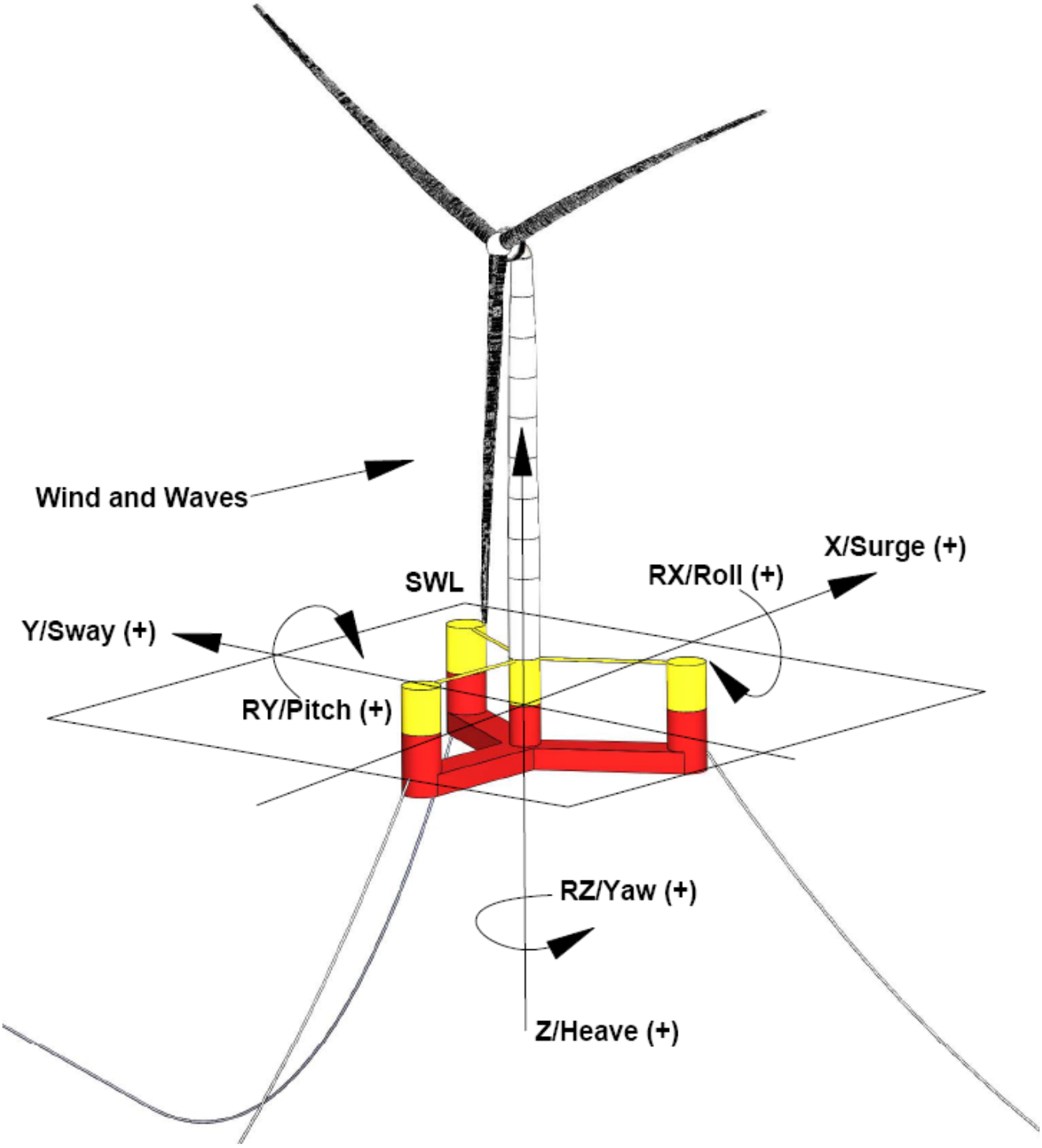

Figure 2. Floating offshore wind turbine reference coordinate system. ***Figure courtesy of the University of Maine***

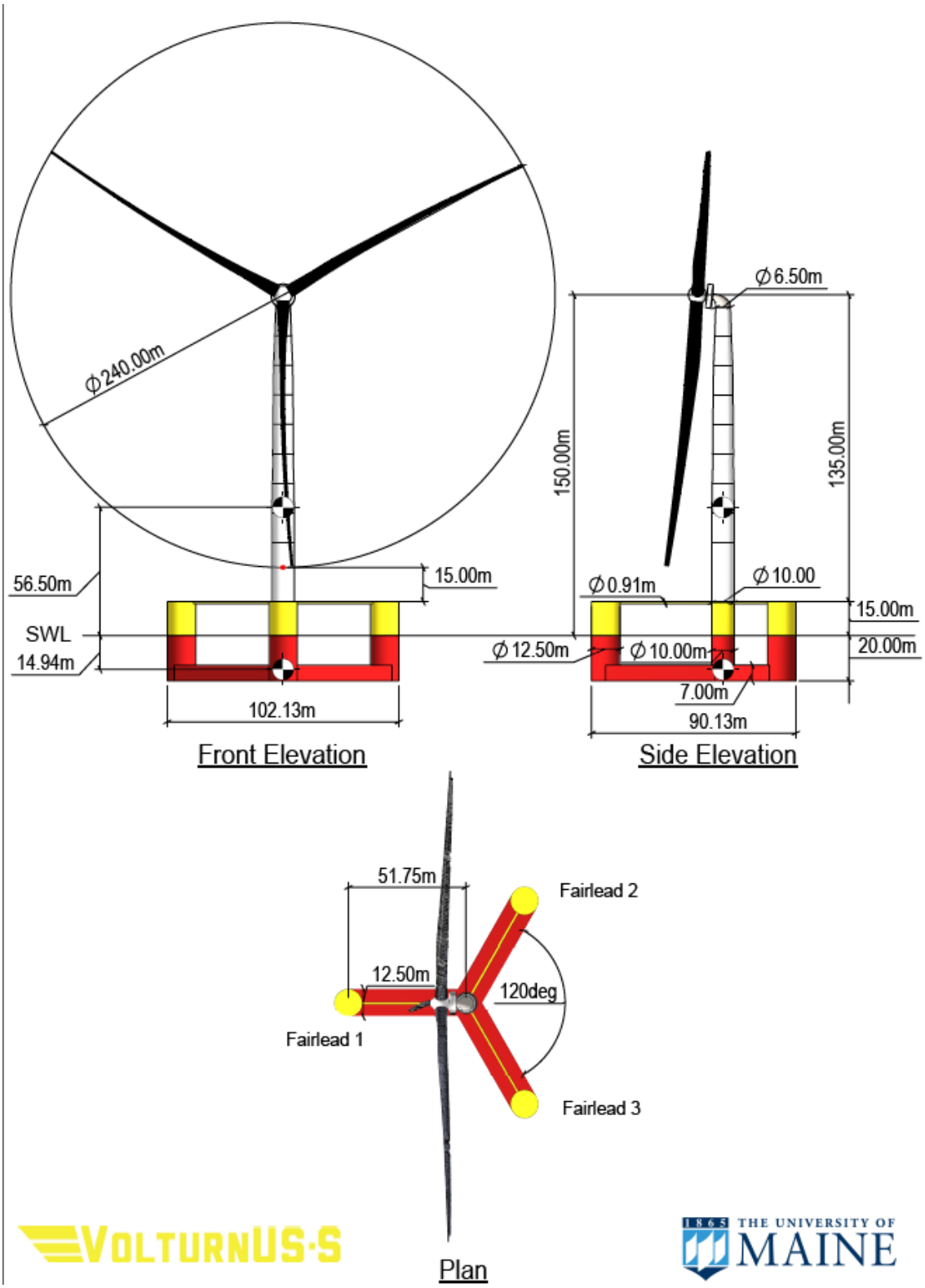

Figure 3. General arrangement. ***Figure courtesy of the University of Maine***

2 Design Details

2.1 UMaine VolturnUS-S Semisubmersible Platform

The reference platform presented in this report is a four-column, steel semisubmersible, and its general properties are provided in Table 2, including system masses, dimensions, centers of gravity and buoyancy, and inertias. Shown in Figure 3, the arrangement of the hull comprises three 12.5-m-diameter buoyant columns radially spaced with centers that are 51.75 m from the tower's vertical axis. The platform-tower interface is atop a fourth buoyant column located at the center of the platform in the surge-sway plane. This central column is connected to the outer columns via three 12.5-m-wide-by-7.0-m-high rectangular bottom pontoons and three 0.9-m-diameter radial struts attached to the bottom and top of the buoyant columns, respectively. When on station, the total mass of the platform is 17,854 t, of which 3,914 t is structural steel, 2,540 t is fixed iron-ore-concrete ballast, divided equally and placed at the base of the three radial columns, 11,300 t is a seawater ballast that floods the majority of the three submerged pontoons, and a 100-t tower interface connection detail. The tower interface was not designed in detail; a point mass of 100 t located at the freeboard was assumed and the connection between the substructure and tower was assumed to be rigid.

Table 2. Semisubmersible Platform Properties

Parameter	Units	Value
Hull Displacement	m^3	20,206
Hull Steel Mass	t	3,914
Tower Interface Mass	t	100
Ballast Mass (Fixed/Fluid)	t	2,540/11,300
Draft	m	20
Freeboard	m	15
Vertical Center of Gravity from SWL	m	-14.94
Vertical Center of Buoyancy from SWL	m	-13.63
Roll Inertia about Center of Gravity	kg-m^2	1.251E+10
Pitch Inertia about Center of Gravity	kg-m^2	1.251E+10
Yaw Inertia about Center of Gravity	kg-m^2	2.367E+10

Representation of the system's hydrodynamic properties in OpenFAST's hydrodynamics module, HydroDyn, uses a potential flow model augmented with a quadratic drag model. Note that in the following section all values are with respect to the platform's reference point, which is defined in OpenFAST as the intersection of the SWL and the tower axis. Frequency-dependent coefficients for the potential flow model were computed using the boundary-element-method hydrodynamics solver WAMIT v6, which solves the first-order hydrostatics, diffraction, and radiation problems, and then uses the resulting response amplitude operators (RAOs) to compute second-order wave-excitation quadratic transfer functions (QTFs) (Lee 1995). Altogether, the WAMIT coefficients account for the platform's properties pertaining to hydrodynamic added mass, wave-radiation damping, hydrostatic restoring, and first-order and second-order wave

forcing. Separately, coefficients for the quadratic drag model account for nonlinear viscous drag effects based on the velocities of the platform as a whole.

The hydrostatic stiffness coefficients evaluated by WAMIT, based on the submerged geometry of the platform, are provided in Table 3. These values are calculated with respect to the platform reference point. Note that the roll and pitch entries in Table 3 represent the restoring moments based only on the water plane area moment of inertia and the system's center of buoyancy. The mass component of each hydrostatic restoring moment is calculated and applied separately within the OpenFAST framework and as such has not been included here.

Table 3. Hull Hydrostatic Stiffness Evaluated by WAMIT (N/m, N/rad or N-m/rad)

	Surge	Sway	Heave	Roll	Pitch	Yaw
Surge	0	0	0	0	0	0
Sway	0	0	0	0	0	0
Heave	0	0	4.470E+06	0	0	0
Roll	0	0	0	2.190E+09	0	0
Pitch	0	0	0	0	2.190E+09	0
Yaw	0	0	0	0	0	0

The hydrodynamic added mass and radiation damping coefficients are provided with respect to platform response frequency in Figure 4. Note that based on previous work with similar symmetry in the surge-sway plane, only the upper off-axis terms have been presented, as the lower terms are identical (Robertson et al. 2014). Additionally, the surge-sway symmetry results in identical values for surge-sway and pitch-roll added mass and damping values, which are overlapped in the figure. In addition to the frequency-dependent added mass, the infinite-frequency added mass coefficients are provided in Table 4.

The radiation damping from the potential flow analysis is applied to the time domain environment of OpenFAST via time convolution of radiation impulse response functions (RdtnMod = 1 in HydroDyn). The convolution formulation captures the memory effect of the hydrodynamic loads associated with radiated waves and was chosen over the alternative state-space formulation based on previous work, which has shown the former method to have greater accuracy for similar systems (Duarte et al. 2013). The impulse response functions, as calculated by WAMIT's F2T utility, are provided in Figure 5. Note that the aforementioned symmetry effects for the added mass values also pertain to the damping properties. Also, all degrees of freedom (DOFs) decay to zero before 45 seconds (s), so the total retained memory time within HydroDyn, RdtnTMax, was conservatively set to 60 s.

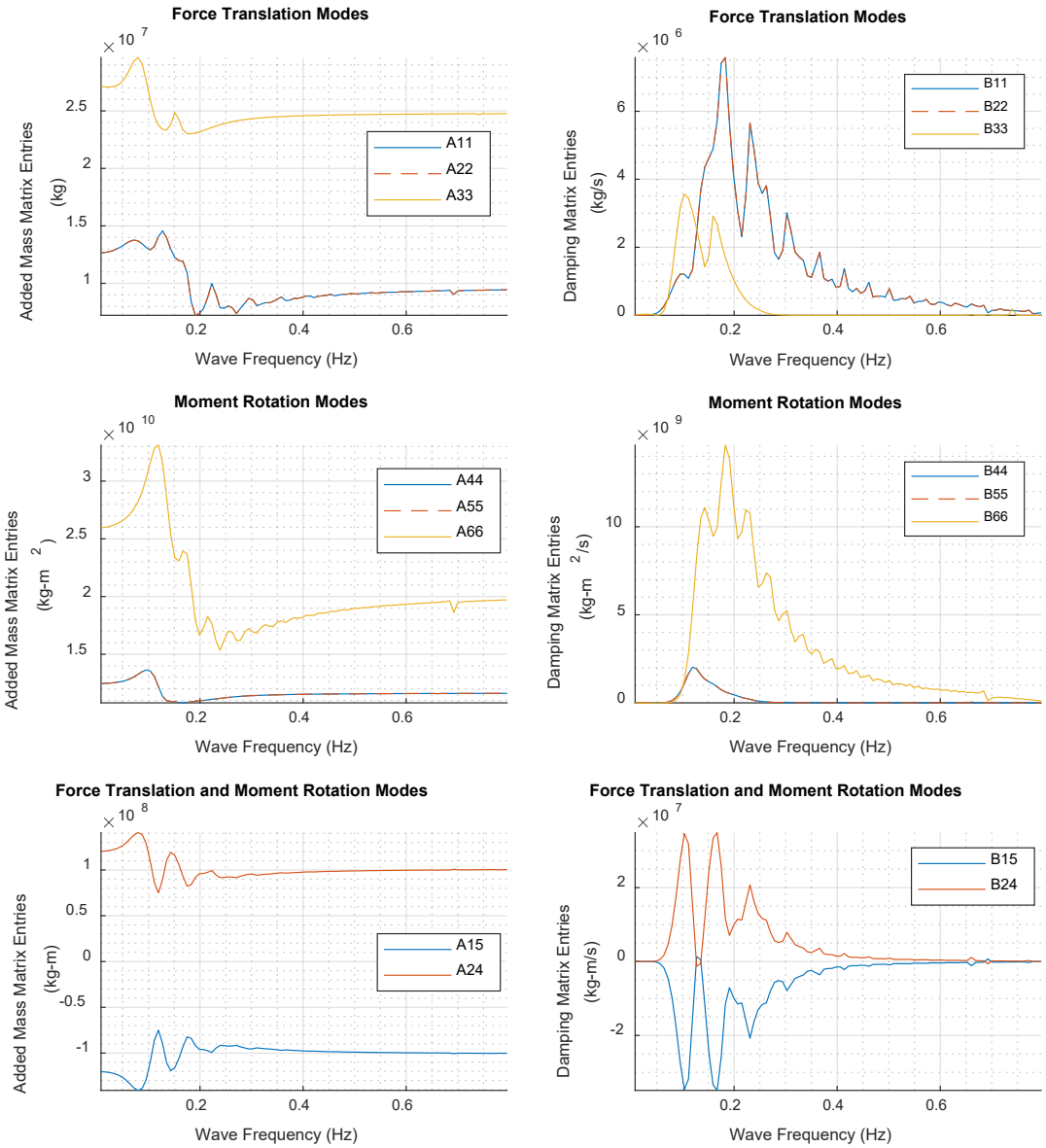

Figure 4. Added mass and radiation damping vs. frequency evaluated by WAMIT

Table 4. Hull Infinite-Frequency Added Mass Evaluated by WAMIT (kg, kg-m or kg-m^2)

	Surge	Sway	Heave	Roll	Pitch	Yaw
Surge	9.640E+06	0	0	0	-1.010E+08	0
Sway	0	9.640E+06	0	1.010E+08	0	0
Heave	0	0	2.480E+07	0	0	0
Roll	0	0	0	1.160E+10	0	0
Pitch	-1.010E+08	0	0	0	1.160E+10	0
Yaw	0	0	0	0	0	2.010E+10

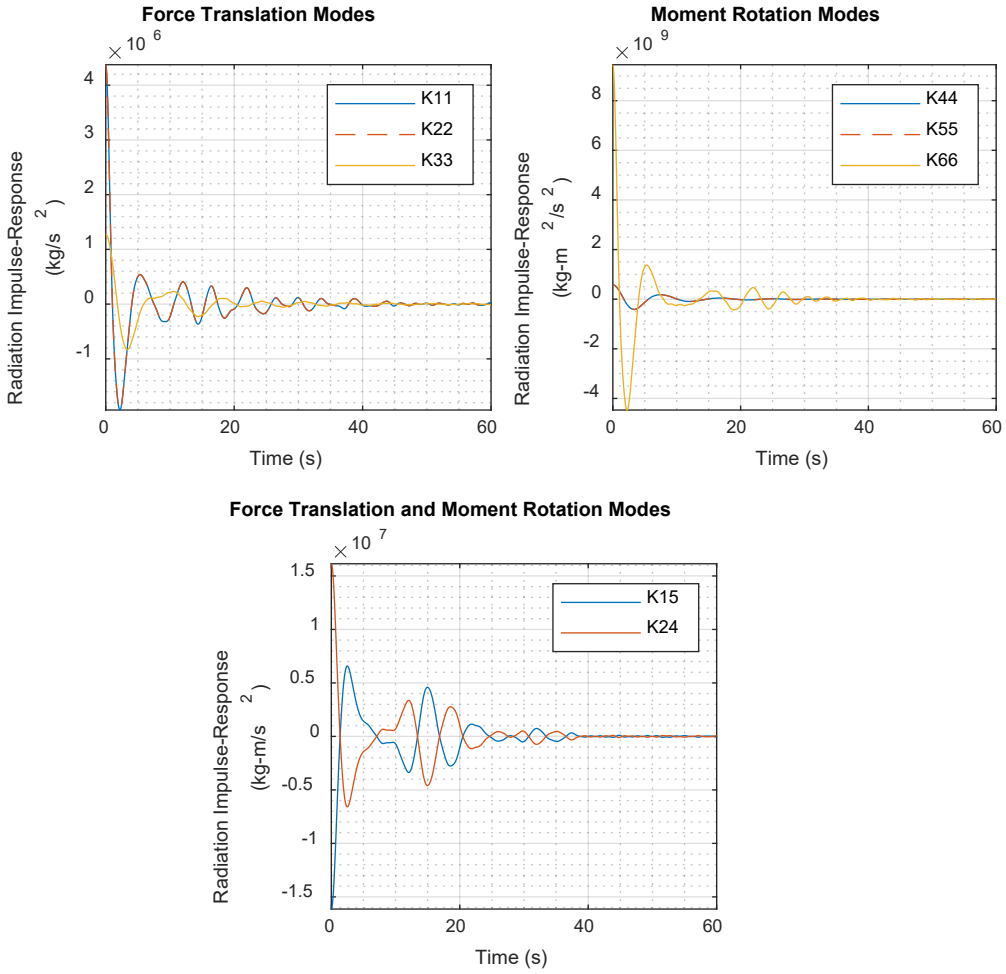

Figure 5. Radiation impulse-response functions

The first-order wave excitation coefficients with respect to wave frequency are provided for a wave heading of 0° in Figure 6. The top left and top right plots are the magnitudes of the translational DOFs and rotational DOFs, respectively. Similarly, the bottom left and bottom right plots depict the phase of the load response for the translational DOFs and rotational DOFs, respectively. Note that values for sway, roll, and yaw have not been provided; as a result of

platform symmetry, the total integrated diffraction loads equate to zero for these DOFs at a wave heading of 0˚.

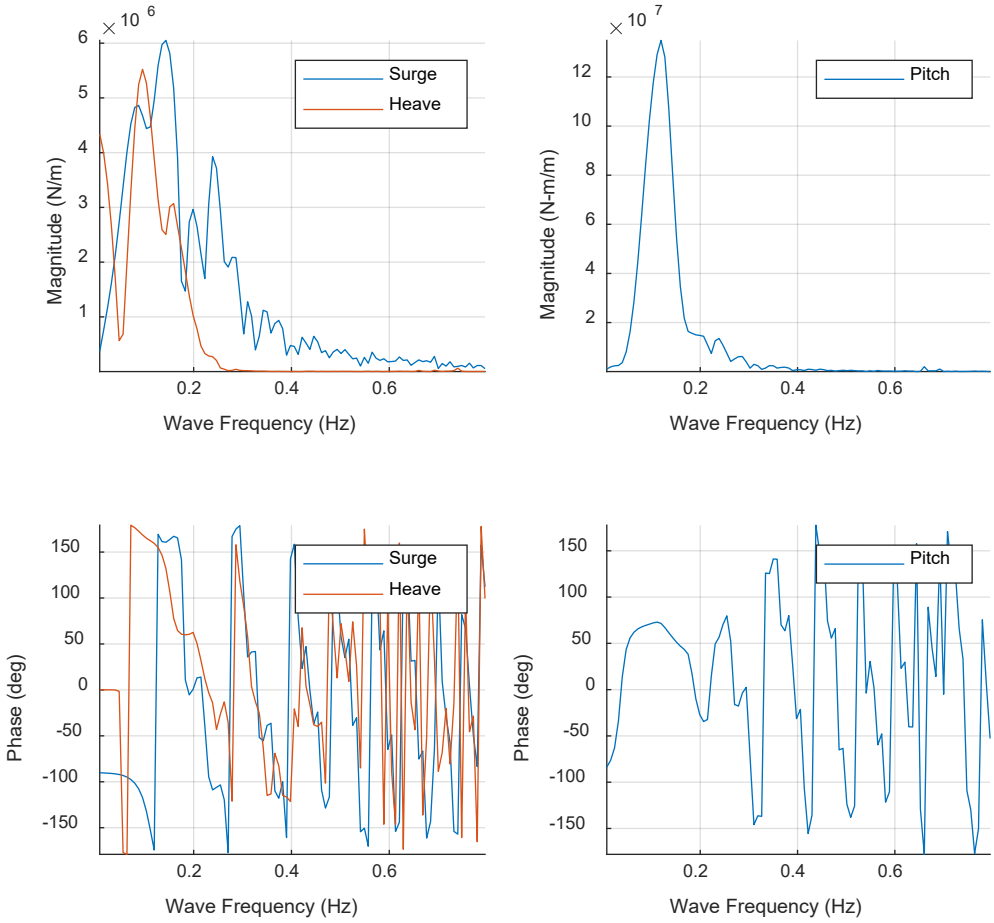

Figure 6. First-order wave excitation coefficients evaluated by WAMIT for a 0˚ wave heading

The second-order QTFs for both sum-frequency and difference-frequency wave excitation are provided in Figure 7 for a wave heading of 0˚, as defined in Figure 2. The response amplitude operators used by WAMIT to generate these QTFs are based on the first-order hydrodynamic coefficients as well as the mass matrix for the full floating system and the linearized mooring stiffness matrix calculated for the platform's undisplaced position—turbine elasticity, aerodynamics, and hydrodynamic viscous drag are neglected. Note that because of the significant increase in the analysis time required to compute the second-order forcing terms, these values have been provided for a wave frequency range of 0.04-0.48 hertz (Hz), with a frequency interval of 0.008 Hz. This array of frequencies captures important difference-frequency (slow drift) loads on the semisubmersible platform, particularly in surge (Chakrabarti 2005), and includes key turbine structural frequencies in its sum-frequency range. When utilizing second-order difference-frequency wave loads, suggested analysis procedures recommend considering wave frequencies up to the peak frequency of the wave field's spectrum (Jonkman et al. forthcoming). As such, the second-order frequency range provided allows analysis of wave fields with peak periods up to 25 s.

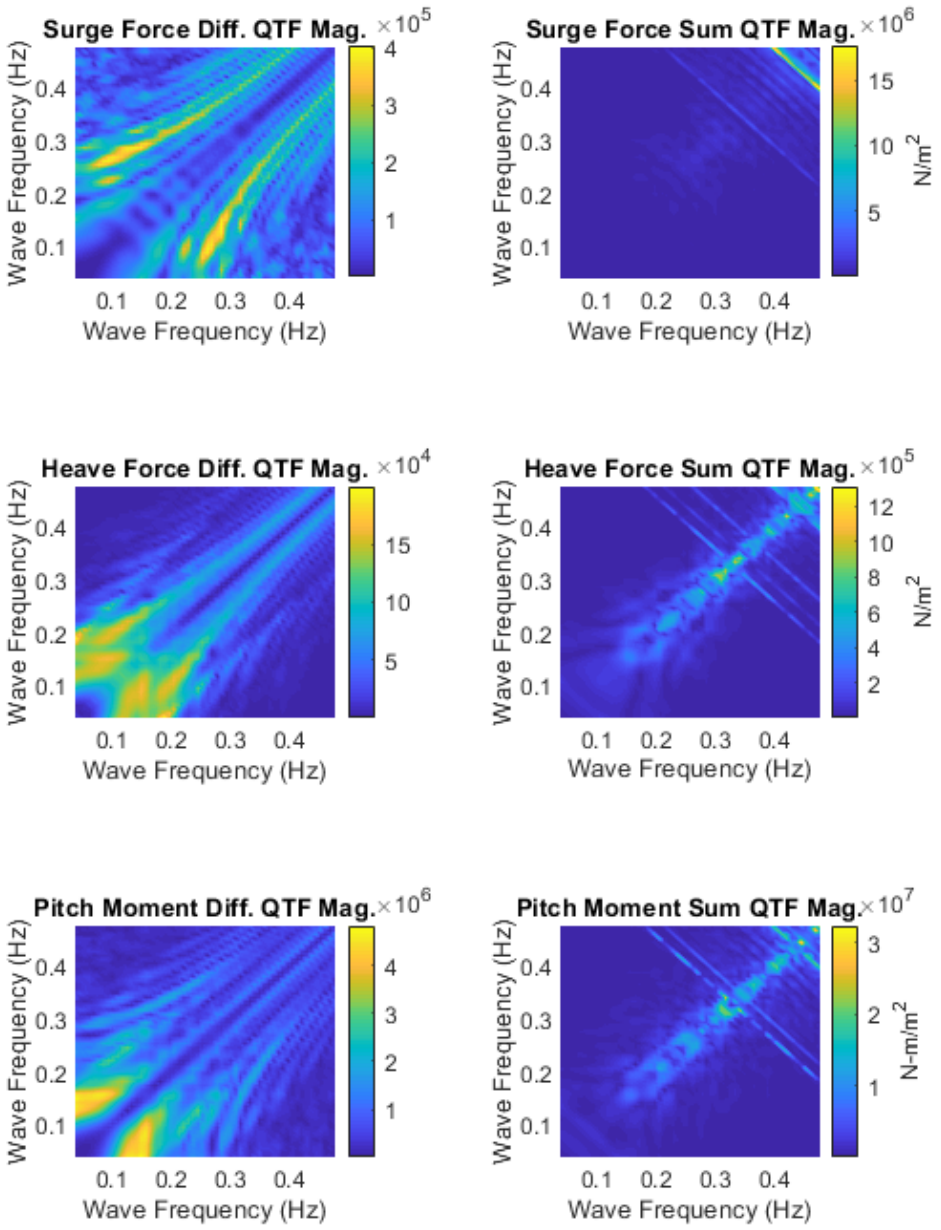

Figure 7. Difference (left) and sum (right) second-order wave forces for a wave heading of 0˚ evaluated by WAMIT

Previous work has identified flow-separation-induced drag to be a large component of the total hydrodynamic damping for a floating offshore wind turbine semisubmersible (Coulling et al. 2013). This additional damping, which is not accounted for in the potential flow model, was represented via the quadratic drag model with coefficients as shown in Table 5. This quadratic drag model is used in conjunction with HydroDyn's linear radiation damping model to represent the platform's total hydrodynamic damping within OpenFAST.

Table 5. Viscous Damping Matrix (N-s^2/m^2, N-s^2, N-s^2/m, N-m-s^2)

	Surge	Sway	Heave	Roll	Pitch	Yaw
Surge	9.225E+05	0	0	0	-8.918E+06	0
Sway	0	9.225E+05	0	8.918E+06	0	0
Heave	0	0	2.296E+06	0	0	0
Roll	0	8.918E+06	0	1.676E+10	0	0
Pitch	-8.918E+06	0	0	0	1.676E+10	0
Yaw	0	0	0	0	0	4.798E+10

The viscous damping model was calculated using OpenFOAM, an open-source computational fluid dynamics code, specifically its steady-state, incompressible solver, SimpleFoam (Greenshields 2011). As shown in Figure 8, a model of the submerged body was built that takes advantage of the platforms symmetry about the y-z plane, as defined in Figure 2. Four unique analyses were run considering the effect of the net drag load on the body due to a unit fluid velocity of either 1 meter per second (m/s) or 1˚/s relative to the platform's surge, heave, roll, and yaw DOFs about the platform reference point. We ran the simulation until a steady-state condition within the domain was achieved, at which point the pressure over the submerged body was integrated with respect to the point concurrent with the tower's vertical axis and the SWL. Based on the assumption of platform symmetry, the sway and pitch terms of the matrix in Table 5 were assumed to be equal in magnitude to those of the surge and roll, respectively. Note that the analysis assumed a kinematic fluid viscosity of 1.5E-06 m^2/s for seawater at 40°F and a fluid density of 1,250 kg/m^3.

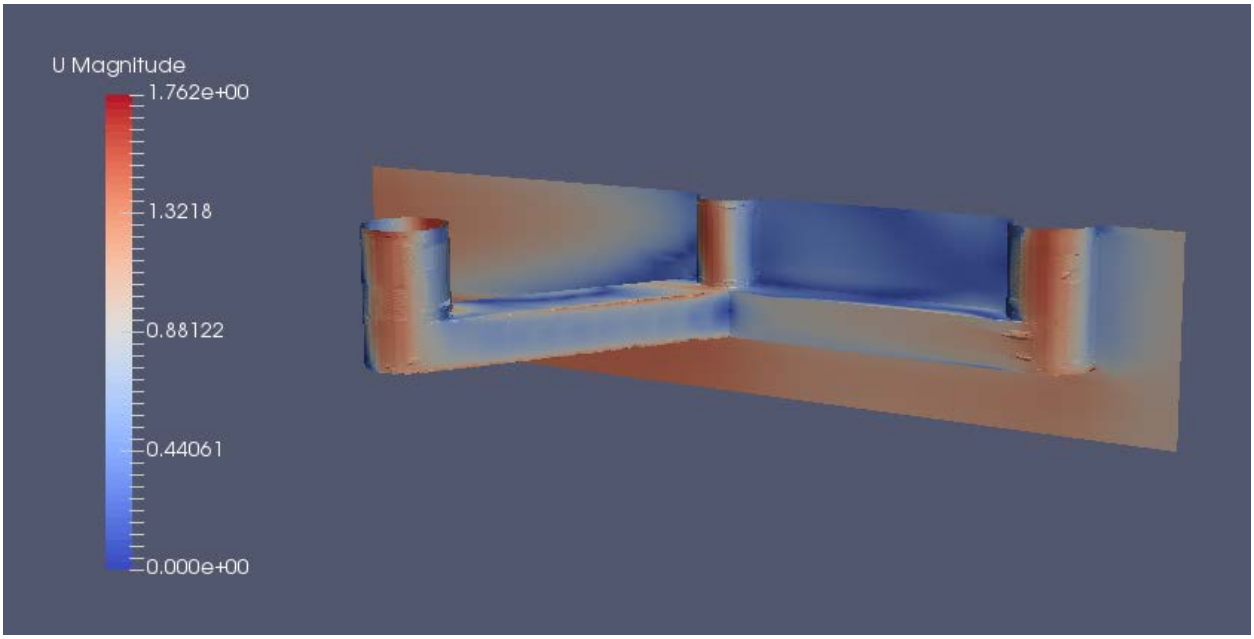

Figure 8. Surge steady-state flow (i.e., flow right to left) drag simulation in OpenFOAM showing the fluid's x-velocity in m/s

2.2 Mooring System Properties

This section presents the design of the UMaine VolturnUS-S chain mooring system. The mooring system properties and arrangement are provided in Table 6 and Figure 9, respectively. The mooring system configuration consists of three 850-m-long chain catenary lines. Each line is connected at the fairlead to one of the platform's three outer columns at a depth of 14 m below the SWL. The lines span radially to anchors spaced equally at 120 degrees in the surge-sway plane, which are located at a depth of 200 m and spaced radially 837.60 m from the tower's centerline. All lines use a studless R3 chain with a nominal (bar) diameter of 185 millimeters (mm). Mooring line drag and added mass coefficients, presented in Table 7, were selected with reference to DNVGL-RP-C205 (Det Norske Veritas 2010)and DNVGL-OS-301 (DNV GL 2015). Note that these coefficients are presented as both the specified value from the aforementioned standards based on the chain nominal diameter, as well as an adjusted value based on the volume-equivalent diameter used in MoorDyn (the diameter of a cylinder having the same volume as the chain, per unit length) (Hall and Goupee 2015).

Table 6. Mooring System Properties

Parameter	Units	Value
Mooring System Type	-	Chain Catenary
Line Type	-	R3 Studless Mooring Chain
Line Breaking Strength	kN	22,286
Number of Lines	-	3
Anchor Depth	m	200
Fairlead Depth	m	14
Anchor Radial Spacing	m	837.6
Fairlead Radial Spacing	m	58
Nominal Chain Diameter	mm	185
Dry Line Linear Density	kg/m	685
Extensional Stiffness	MN	3270
Line Unstretched Length	m	850
Fairlead Pretension	kN	2,437
Fairlead Angle from SWL	°	56.4

Table 7. Mooring Line Drag and Added Mass Coefficients

Mooring Line Coefficients	Relative to Chain Nominal Diameter	Relative to Volume-Equivalent Diameter
Normal Added Mass	1	0.82
Tangential Added Mass	1	0.27
Normal Drag	2	1.11
Tangential Drag	1.15	0.20

The chain size was selected based on a desire to keep the system's peak surge-sway offset under 25 m during normal operational conditions to limit design constraints on a dynamic electrical umbilical. Though the chain size meets the strength requirements based on the peak fairlead tension loads presented in Section 4, fatigue analysis of the lines has not been performed. It should be noted that the size of the chain specified for this design is representative of the largest mooring chain currently available at the time of this publishing. Because of limitations of chain size availability and handling vessel capacity, fully designed mooring systems for a 15-MW floating offshore wind turbine could potentially be quite different. Further advances in mooring system technology, such as the use of synthetic materials, will likely be required to optimize a mooring system of this scale.

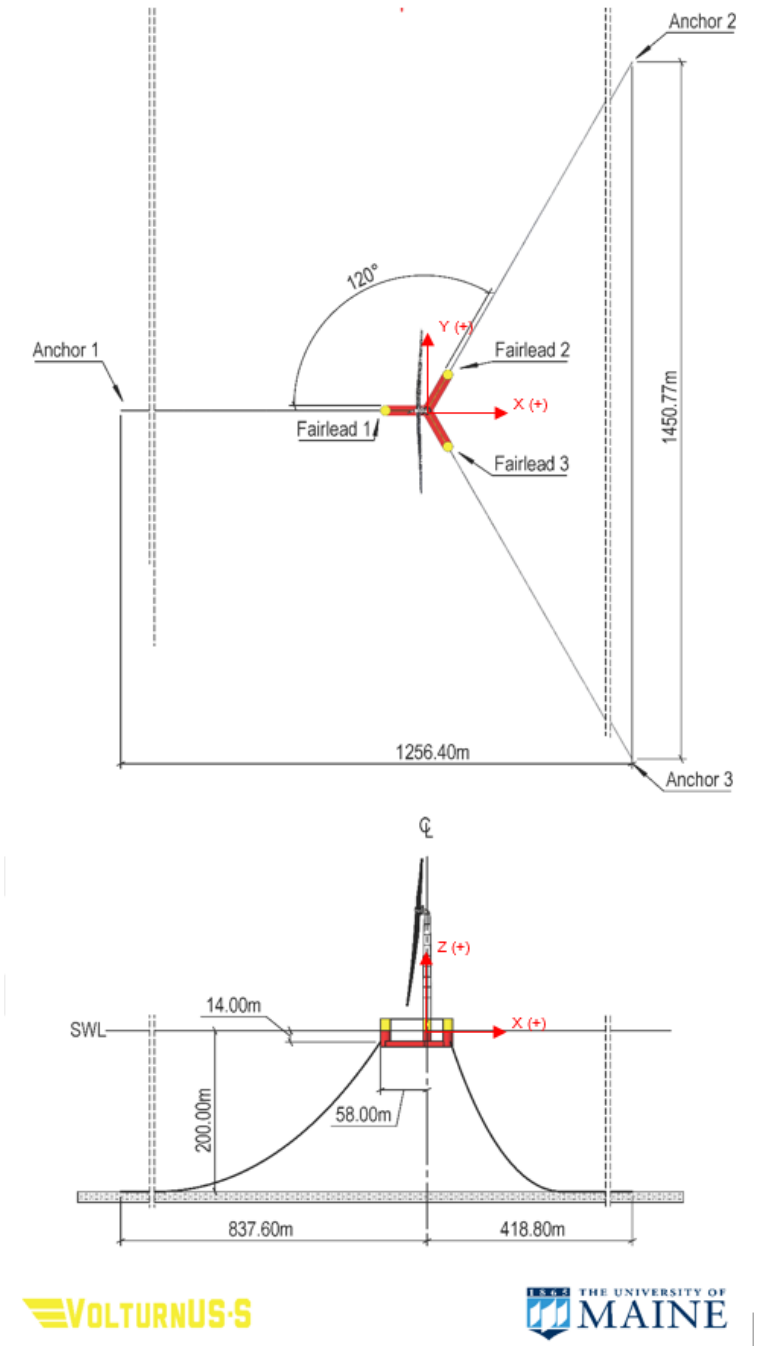

Figure 9. Mooring system arrangement within the inertia frame shown in plan (top) and elevation (bottom) views. *Figure courtesy of the University of Maine*

2.3 Floating Tower

Floating offshore wind turbine towers have higher stiffness requirements than fixed-bottom configurations because of the increased inertial and gravity loads resulting from platform motion. The tower for this semisubmersible configuration was designed separate from the monopile configuration previously described (Gaertner et al. 2020). The tower was designed as an isotropic steel tube using the Wind-Plant Integrated System Design & Engineering Model

(WISDEM®) (National Renewable Energy Laboratory [NREL] 2020a) and BModes v1.03 (Bir 2005), with free-free boundary conditions.

Frequency considerations were the most important constraints on the tower design. Operation design load cases (DLCs) of the floating platform show higher variability in the rotor rotation speeds brought on by platform motion, coupled with the high rotor inertia and a relatively low maximum blade pitch rate at 2°/s. The higher rotor speed variability increased instances of rotor under and overspeeding beyond the design 5- to 7.56-rpm operating range. To avoid potential tower resonance issues, the tower was conservatively designed to have the first fore-aft and side-side natural frequencies outside modified rotation speed (1P) and blade passing (3P) ranges, taking the increased rotor speed variability into account. The design constraining operational rotor speed (Ω_{const}) range was determined to be 3.97 to 8.86 revolutions per minute (rpm). These values were derived from Eq. 1 and 2, which bound the minimum and maximum rotor speeds as a function of wind speed (U) and two standard deviations of the variability observed in all operational DLCs. A stiff-stiff tower, with 1st natural frequencies above 3P, was required because of the very narrow soft-stiff range between 1P and 3P (shown in Figure 10) when additional safety factors are applied.

$$\Omega_{const,min} = \min[\bar{\Omega}(U) - 2\Omega_{std}(U)] \quad (1)$$

$$\Omega_{const,max} = \max[\bar{\Omega}(U) + 2\Omega_{std}(U)] \quad (2)$$

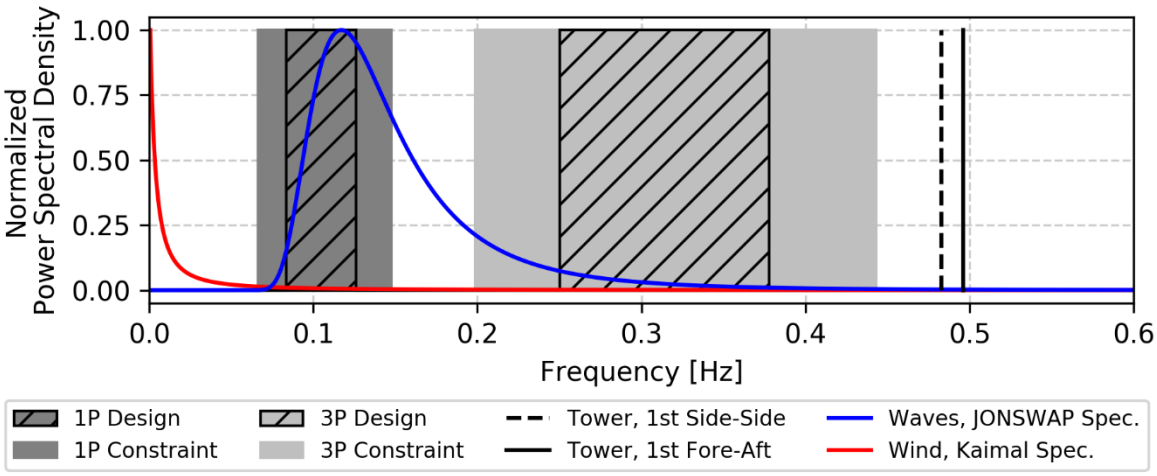

Figure 10. Tower natural frequencies relative to excitation frequencies

We chose the same tower base height (15 m) and hub height (150 m) as the monopile configuration, resulting in a total flexible tower length of 129.495 m. The design was constrained to have a maximum outer diameter of 10 m and a 6.5-m tower-top diameter to interface with the existing nacelle bedplate design. The stiffer semisubmersible tower has a mass of 1,263 t, 47% greater than the tower for the monopile configuration. The tower properties are summarized in Table 8 and the steel material properties are given in Table 9.

Table 8. Floating Tower Properties

Parameter	Value	Units
Mass	1,263	ton
Length	129.495	m
Base Outer Diameter	10	m
Top Outer Diameter	6.5	m
1st Fore-Aft Bending Mode	0.496	Hz
1st Side-Side Bending Mode	0.483	Hz

Table 9. Steel Material Properties for the Floating Tower

Parameter	Symbol	Value	Units
Young's Modulus	E	200e11	Pascals (Pa)
Shear Modulus	G	793e10	Pa
Density	ρ	785e3	kg/m^3

The tower dimensions as a function of height are shown in Figure 11 and listed in Table 10. From these properties, the elastic cross-sectional properties needed for aeroelastic modeling tools like OpenFAST can easily be calculated (see Appendix B in Gaertner et al. [2020]) and are also shown in Figure 11.

Table 10. Tower Dimensions as a Function of Height

Height [m]	Outer Diameter [m]	Thickness [mm]
15.000	10.000	82.954
28.000	9.964	82.954
28.001	9.964	83.073
41.000	9.967	83.073
41.001	9.967	82.799
54.000	9.927	82.799
54.001	9.927	29.900
67.000	9.528	29.900
67.001	9.528	27.842
80.000	9.149	27.842
80.001	9.149	25.567
93.000	8.945	25.567
93.001	8.945	22.854
106.000	8.735	22.854
106.001	8.735	20.250
119.000	8.405	20.250
119.001	8.405	18.339
132.000	7.321	18.339
132.001	7.321	21.211
144.582	6.500	21.211

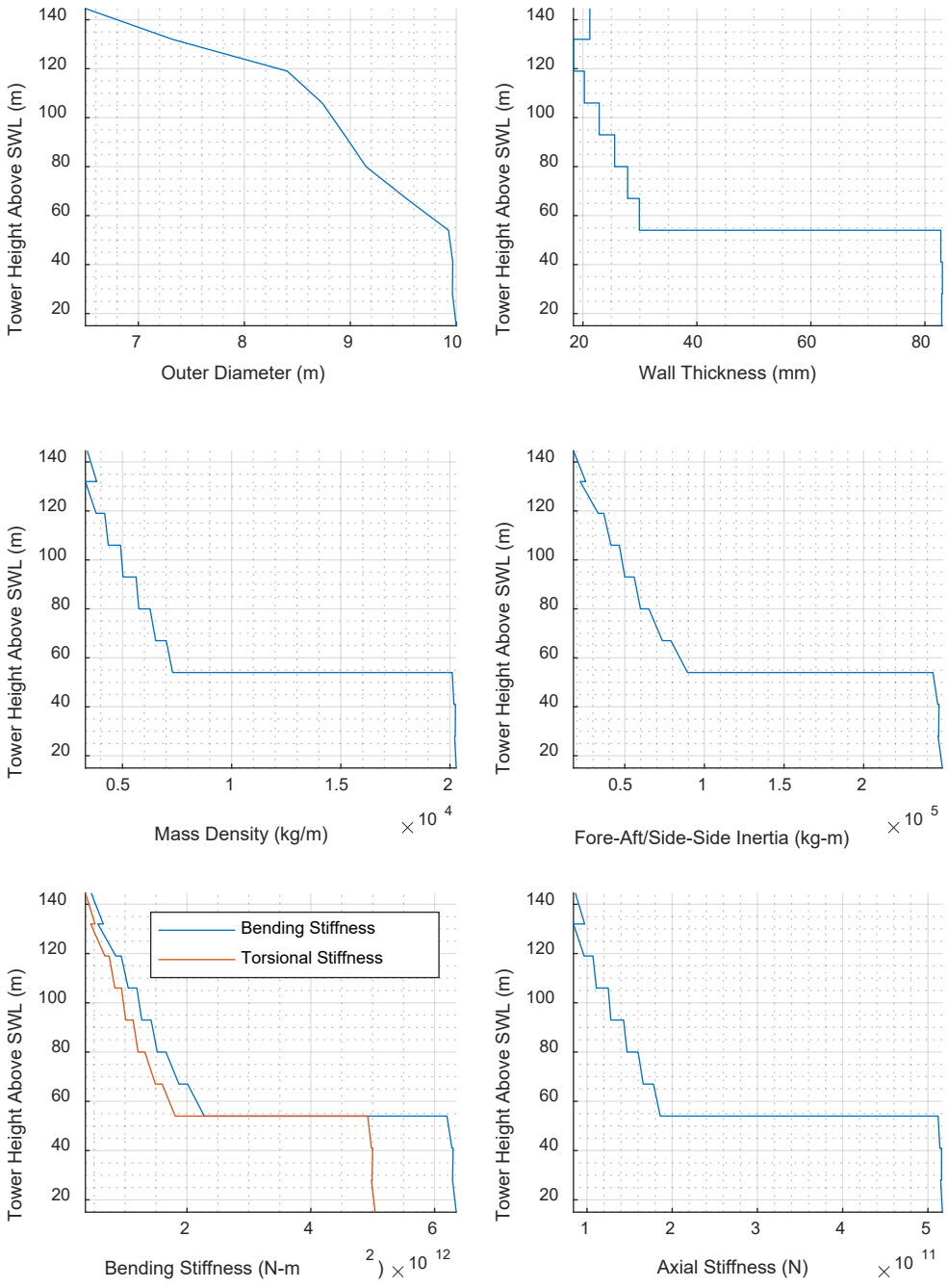

Figure 11. Tower structural properties vs. tower height above SWL

2.4 Wind Turbine Controller

The same control strategy as the IEA Wind 15-MW reference turbine monopile configuration was implemented with some minor adaptations to account for floating platform dynamics. The NREL Reference Open Source Controller (ROSCO) (NREL 2020b) is still used, with a minimum rotor speed of 5 rpm and a rated rotor speed of 7.55 rpm. A blade pitch setting of 0˚ is used when operating at the design tip-speed ratio (TSR=9.0) in Region 2.

For tuning of the standard blade pitch and generator torque controllers, we modified the target pitch controller damping ratio and natural frequency to 1.0 and 0.2 radians per second (rad/s), respectively. The torque controller target damping ratio and natural frequency were also changed to 0.85 and 0.12 rad/s, respectively. Additionally, the tower-top fore-aft motion is multiplied times a proportional feedback term and added to the pitch controller command signal. This term was found to be -9.32196 s using the ROSCO generic tuning logic. The tower-top fore-aft motion signal is filtered through a second-order low-pass filter and a notch filter. The second-order low-pass filter has a cutoff frequency at the platform pitching natural frequency of 0.213 rad/s and a damping ratio of 1.0. The notch filter is centered at the tower fore-aft natural frequency of 3.12 rad/s and has a Q factor of 2.0.

3 System Identification

3.1 Static Surge-Sway Offsets

This section presents fairlead and anchor tension values resulting from static offsets of the system in the surge-sway plane. The fairlead and anchor tensions in Figure 12 demonstrate the nonlinear restoring force associated with the catenary mooring system. We conducted the OpenFAST simulations by setting the platform displacements at various surge-sway points and holding platform DOFs constant. The simulation was then run for 150 s to bypass transient cable motions at the start of the analysis and to allow the mooring lines to establish an equilibrium position. The fairlead tensions presented here were recorded from the last time step in each simulation. Note that the anchor and fairlead numbering is with respect to Figure 9.

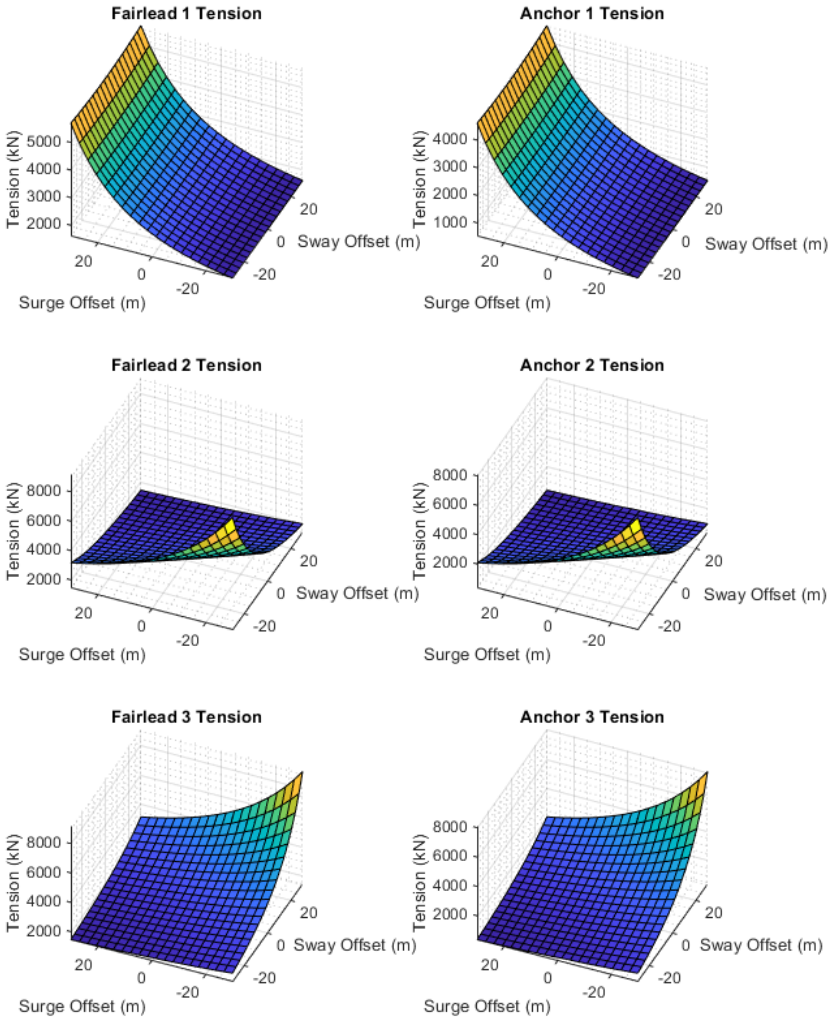

Figure 12. Fairlead and anchor tension vs. surge-sway offset

3.2 Rigid-Body Free Decays

We conducted free-decay simulations in OpenFAST for each of the rigid-body DOFs. The results of the free-decay tests are presented in Figure 13 through Figure 16 and depict the time history of the decay as well as the logarithmic decrement of the decay signal. Note the effect of the quadratic damping model, discussed in Section 2.1, is observed in each DOF and is represented by the slope of the logarithmic decrement trend. The simulations considered a still wind environment and though aerodynamic drag was considered in the simulation, its effects were minimized by orienting the blades such that, based on the motion of the decay, they produced minimal drag. The decay simulations considered all DOFs pertaining to the platform, tower, and blades. The natural frequencies of the rigid-body modes of the system, summarized in Table 11, were calculated by taking the average period of oscillation over the decays shown in the following figures.

Table 11. Rigid-Body Natural Frequencies

Rigid-Body Model	Value	Units
Surge	0.007	Hz
Sway	0.007	Hz
Heave	0.049	Hz
Roll	0.036	Hz
Pitch	0.036	Hz
Yaw	0.011	Hz

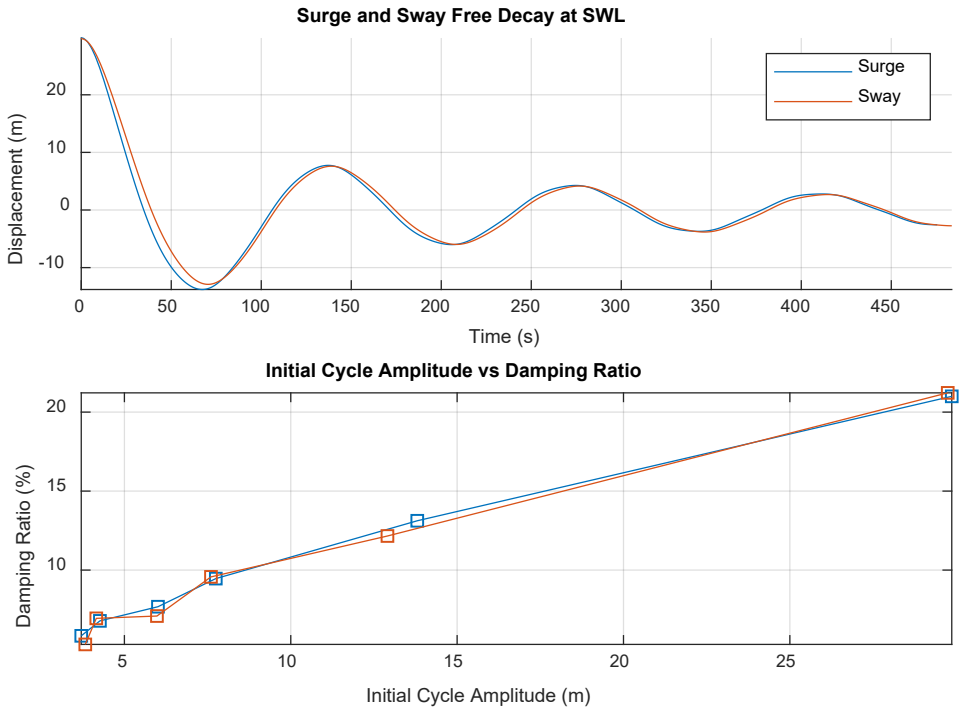

Figure 13. SWL surge and sway free-decay time histories (top) and damping ratio vs. initial cycle amplitude (bottom)

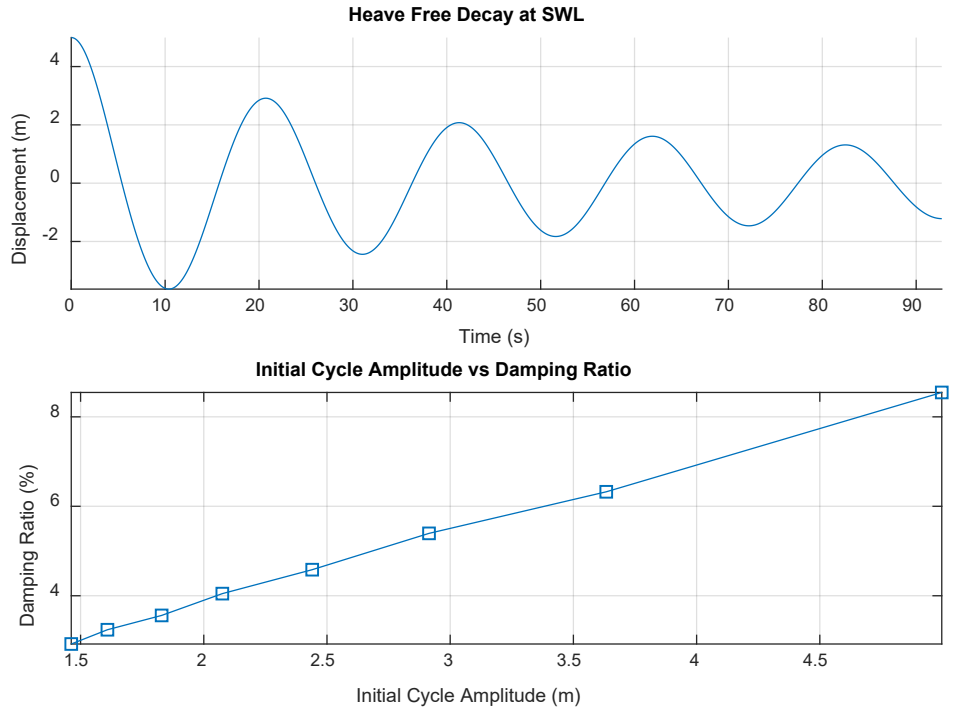

Figure 14. SWL heave free-decay time histories (top) and damping ratio vs. initial cycle amplitude (bottom)

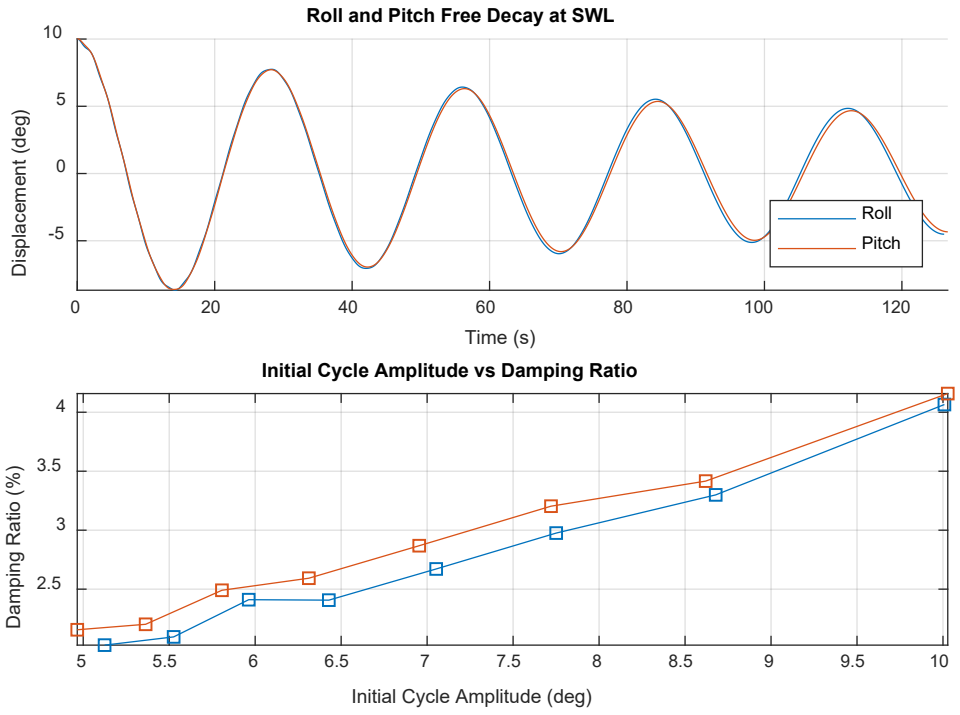

Figure 15. SWL pitch and roll free-decay time histories (top) and damping ratio vs. initial cycle amplitude (bottom)

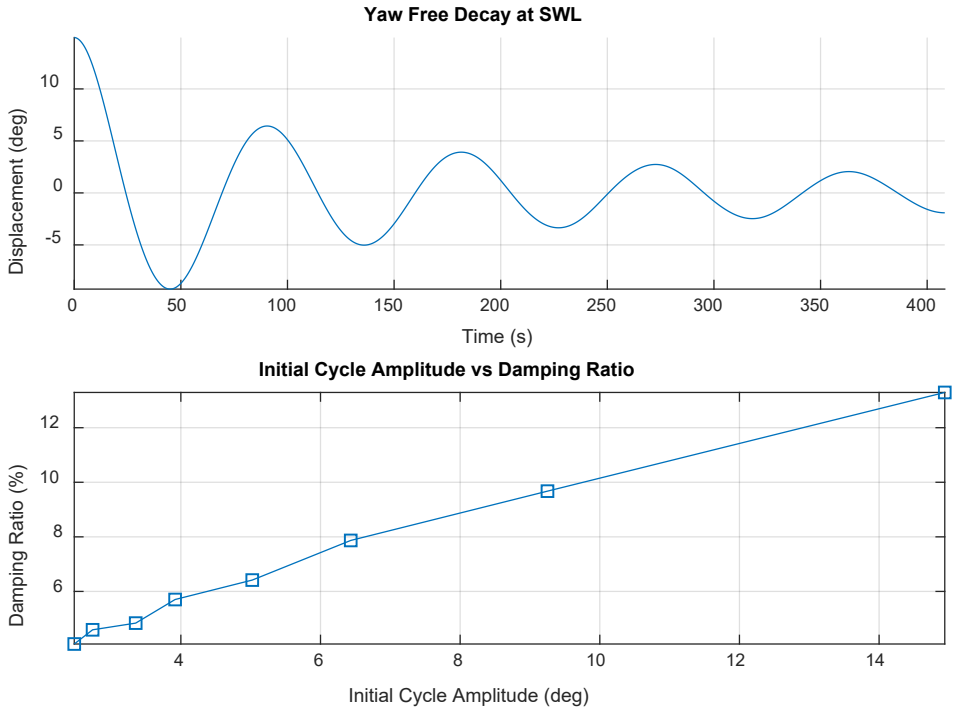

Figure 16. SWL yaw free-decay time histories (top) and damping ratio vs. initial cycle amplitude (bottom)

3.3 Response Amplitude Operators

This section presents the analysis results for the floating offshore wind turbine's rigid-body wave-induced motion RAOs. We evaluated the RAOs via regular wave simulations of 5,000 s conducted at wave periods from 2.5 s to 30 s in 0.25-s increments considering a wave heading of 0˚, as defined in Figure 2. For this effort, we disabled OpenFAST's AeroDyn module; therefore, the effects of aerodynamic loading were not considered in this analysis. Additionally, we disabled the DOFs pertaining to the tower, nacelle, hub, and blades for these simulations. Two wave amplitudes of 2 m and 8 m were analyzed to better understand the effect of the nonlinear damping effect. As can be observed from the RAO magnitude response, this effect is only present at wave frequencies aligned with a rigid-body natural frequency of the system.

For a wave heading of 0˚, only the RAOs relating to surge, heave, and pitch were considered, shown respectively in Figure 17, Figure 18, and Figure 19. The orientation of the floating offshore wind turbine was defined symmetrically about the x-axis, as shown in Figure 2; therefore, when considering a wave angle of 0˚ or 180˚ the forces in sway, roll, and yaw are symmetric about the surge-heave plane yielding a net force or moment of zero. This effectively creates a RAO of zero at all wave frequencies for the DOFs of sway, roll, and yaw in this wave heading.

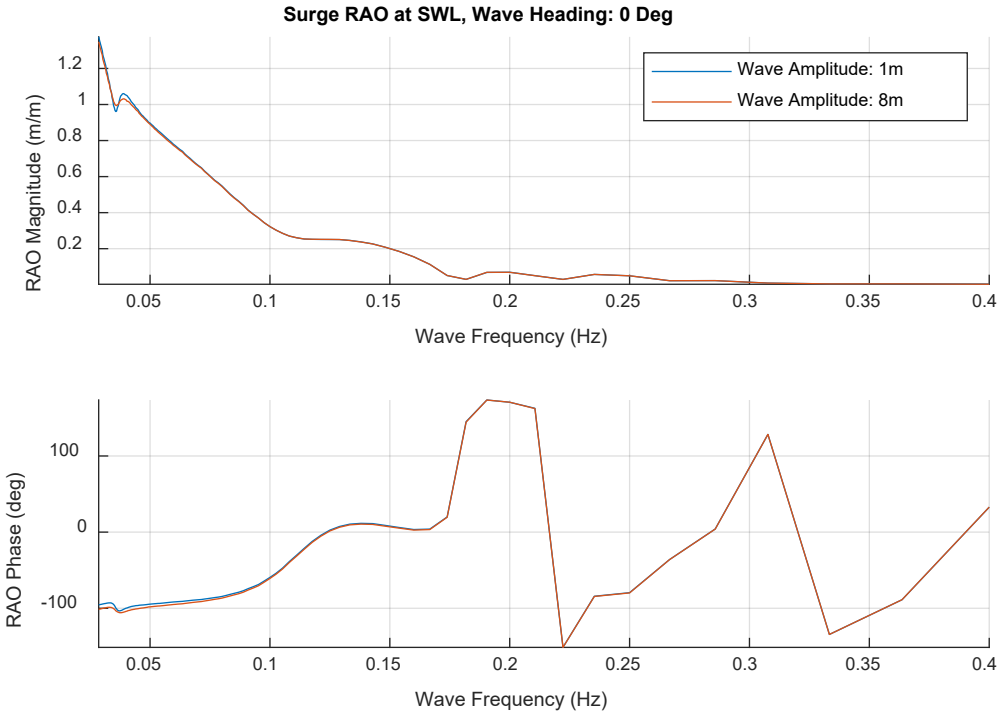

Figure 17. SWL surge RAO magnitude (top) and phase (bottom)

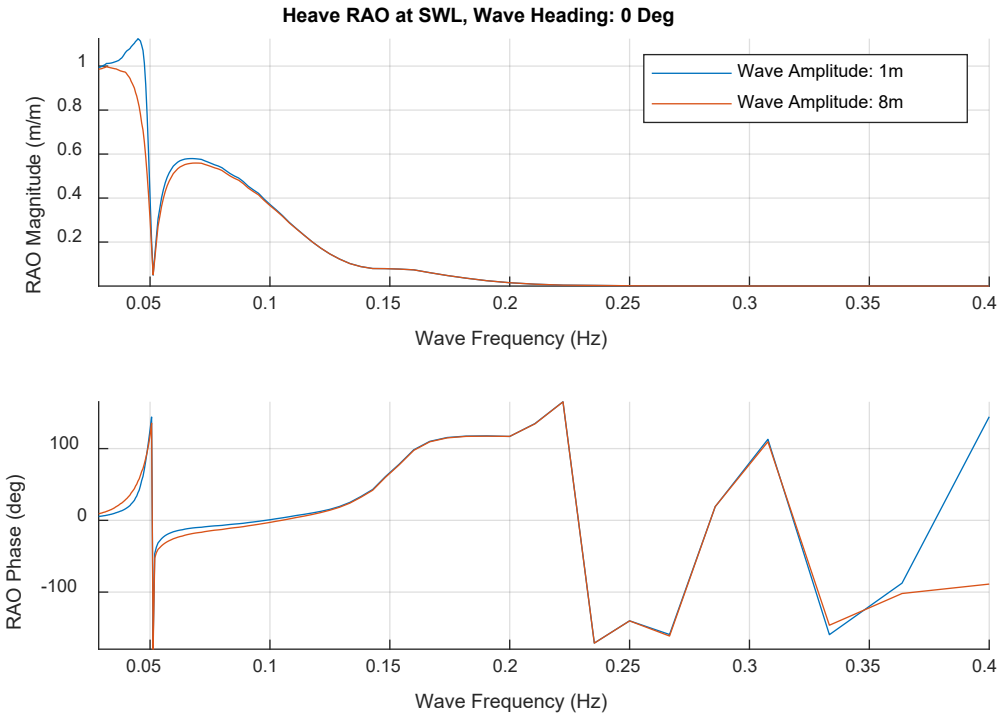

Figure 18. SWL heave RAO magnitude (top) and phase (bottom)

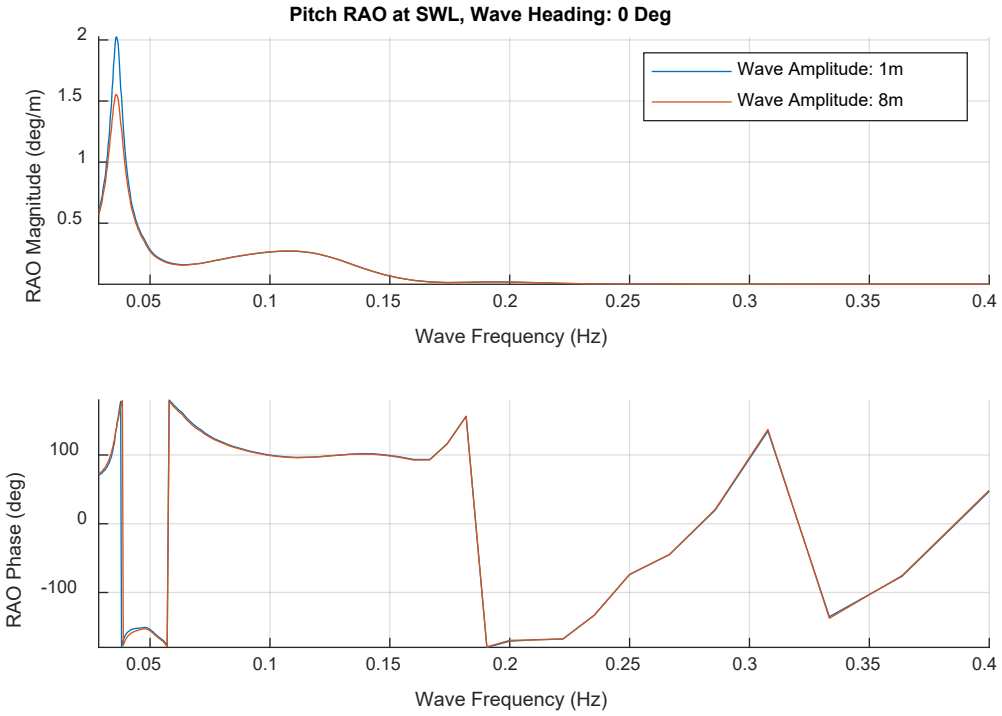

Figure 19. SWL pitch RAO magnitude (top) and phase (bottom)

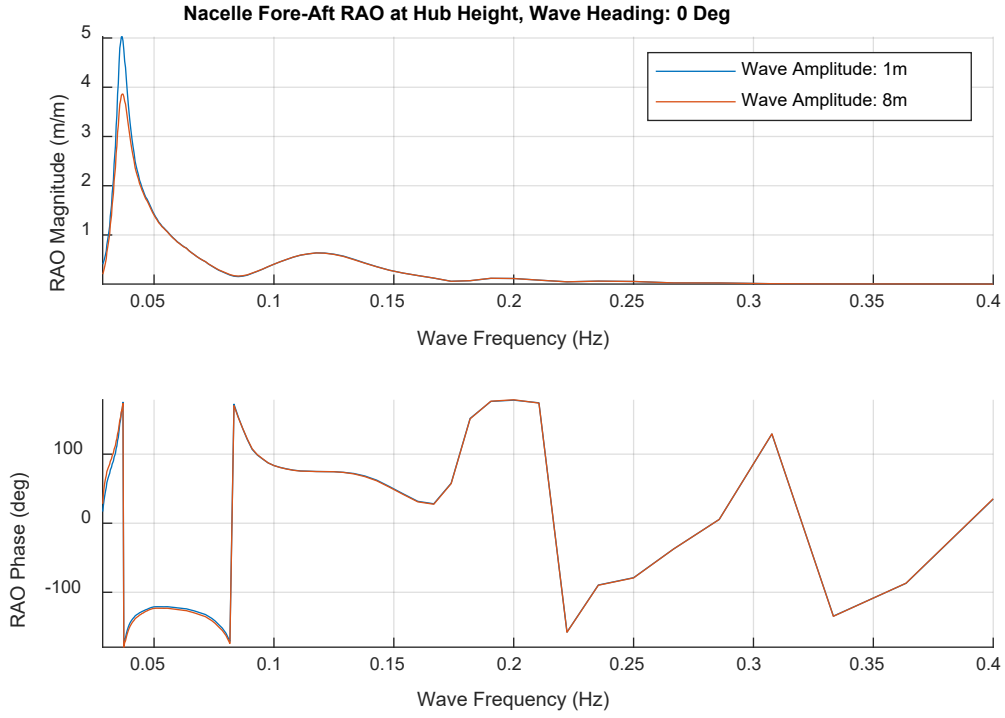

Figure 20. RNA fore-aft RAO magnitude (top) and phase (bottom)

4 System Performance Assessment

A subset of IEC design load case conditions was selected to gauge the performance of the reference floating offshore wind turbine in the presence of representative normal and extreme design conditions (IEC 61400-1 [2020]). The list of simulations considered for analysis in OpenFAST is provided in Table 12 and the simulations were selected to represent governing conditions of various critical components of the floating offshore wind turbine based on design experience of similar systems. Note that all conditions considered an aligned wind and wave heading of 0˚, as defined by Figure 2. The environmental conditions associated with the design cases are representative of the U.S. East Coast, as defined in Stewart et al. (2015)and Viselli et al. (2015c).

The floating offshore wind turbine's performance under these design conditons is summarized via statistics for various outputs grouped by acceleration in Figure 21, deflections and displacements in Figure 22, moments in Figure 23, and forces in Figure 24. Labeling in the following figures represents the nomenclature used to describe OpenFAST outputs. Definitions of these values have been provided in Table 13. Key observations from these results include the following:

- General turbine performance in a floating offshore wind turbine application is often gauged by expected maximum platform pitch angles and accelerations observed at the RNA. Considering the floating offshore wind turbine's acceleration results in Figure 21, it can be observed that the peak acceleration occuring during DLC 6.3 was found to be less and 1.5 m/s^2. Additionally, as shown in Figure 22, the peak platform pitch angle has been limited to less than 6˚.
- The maximum blade tip deflection, as shown in Figure 22, does not exceed values reported in the monopile design of the IEA-15-240-RWT (Gaertner et al. 2020). As such, excessive blade deflection attributed to platform pitch angle was not observed.
- Regarding the mooring system, Figure 22 indicates that the platform did not exceed a surge-sway offset of 25 m, which satifies the aforementioned design requirement. Additionally, the peak fairlead tension was found to be less than the breaking strength of the chain.

Table 12. IEC Design Load Case Matrix

DLC	Wind Condi-tion	Hub Height Wind Speed (m/s)	Wind Headings (°)	Significant Wave Height (m)	Peak Period (s)	Gamma Shape Factor (-)	Wave Headings (°)	Settings	# of Seeds	Total # of Sims.
1.1	NTM	4.00	0.00	1.10	8.52	1.00	0.00	-	6	6
		6.00	0.00	1.18	8.31	1.00	0.00	-	6	6
		8.00	0.00	1.32	8.01	1.00	0.00	-	6	6
		10.00	0.00	1.54	7.65	1.00	0.00	-	6	6
		12.00	0.00	1.84	7.44	1.00	0.00	-	6	6
		14.00	0.00	2.19	7.46	1.00	0.00	-	6	6
		16.00	0.00	2.60	7.64	1.35	0.00	-	6	6
		18.00	0.00	3.06	8.05	1.59	0.00	-	6	6
		20.00	0.00	3.62	8.52	1.82	0.00	-	6	6
		22.00	0.00	4.03	8.99	1.82	0.00	-	6	6
		24.00	0.00	4.52	9.45	1.89	0.00	-	6	6
1.3	ETM	4.00	0.00	1.10	8.52	1.00	0.00	-	6	6
		6.00	0.00	1.18	8.31	1.00	0.00	-	6	6
		8.00	0.00	1.32	8.01	1.00	0.00	-	6	6
		10.00	0.00	1.54	7.65	1.00	0.00	-	6	6
		12.00	0.00	1.84	7.44	1.00	0.00	-	6	6
		14.00	0.00	2.19	7.46	1.00	0.00	-	6	6
		16.00	0.00	2.60	7.64	1.35	0.00	-	6	6
		18.00	0.00	3.06	8.05	1.59	0.00	-	6	6
		20.00	0.00	3.62	8.52	1.82	0.00	-	6	6
		22.00	0.00	4.03	8.99	1.82	0.00	-	6	6
		24.00	0.00	4.52	9.45	1.89	0.00	-	6	6
1.4	ECD+/-R-2.0	8.00	0.00	1.32	8.01	1.00	0.00	+/- Dir. Change	1	2
	ECD+/-R	10.00	0.00	1.54	7.65	1.00	0.00	+/- Dir. Change	1	2
	ECD+/-R+2.0	12.00	0.00	1.84	7.44	1.00	0.00	+/- Dir. Change	1	2
1.6	NTM	4.00	0.00	6.30	11.50	2.75	0.00	-	6	6
		6.00	0.00	8.00	12.70	2.75	0.00	-	6	6
		8.00	0.00	8.00	12.70	2.75	0.00	-	6	6
		10.00	0.00	8.10	12.80	2.75	0.00	-	6	6
		12.00	0.00	8.50	13.10	2.75	0.00	-	6	6
		14.00	0.00	8.50	13.10	2.75	0.00	-	6	6
		16.00	0.00	9.80	14.10	2.75	0.00	-	6	6
		18.00	0.00	9.80	14.10	2.75	0.00	-	6	6
		20.00	0.00	9.80	14.10	2.75	0.00	-	6	6
		22.00	0.00	9.80	14.10	2.75	0.00	-	6	6
		24.00	0.00	9.80	14.10	2.75	0.00	-	6	6
6.1	EWM 50 yr	47.50	0.00	10.70	14.20	2.75	0.00	Yaw +/- 8°	6	12
6.3	EWM 1 yr	38.00	0.00	6.98	11.70	2.75	0.00	Yaw +/- 20°	6	12

NTM normal turbulence model
ETM extreme turbulence model
ECD extreme coherent gust with direction change
EWM extreme wind speed model

Table 13. OpenFAST Output Definitions

OpenFAST Output Name	Description
RootMxb1	Blade 1 edgewise moment (i.e., the moment caused by edgewise forces) at the blade root
RootMyb1	Blade 1 flapwise moment (i.e., the moment caused by flapwise forces) at the blade root
TipDxb1	Blade 1 flapwise tip deflection (relative to the pitch axis)
TipDyb1	Blade 1 edgewise tip deflection (relative to the pitch axis)
NcIMUTAxs	Nacelle inertial measurement unit translational acceleration in the x direction(absolute)
NcIMUTAys	Nacelle inertial measurement unit translational acceleration in the y direction(absolute)
NcIMUTAzs	Nacelle inertial measurement unit translational acceleration in the z direction(absolute)
YawBrTDxt	Tower top/yaw bearing fore-aft (translational) deflection (relative to the undeflected position)
YawBrTDyt	Tower top/yaw bearing side-to-side (translational) deflection (relative to the undeflected position)
TwrBsMxt	Tower base roll (or side-to-side) moment (i.e., the moment caused by side-to-side forces)
TwrBsMyt	Tower base pitching (or fore-aft) moment (i.e., the moment caused by fore-aft forces)
PtfmSurge	Platform horizontal surge (translational) displacement
PtfmHeave	Platform vertical heave (translational) displacement
PtfmPitch	Platform pitch tilt angular (rotational) displacement
FAIRTEN1	Fairlead tension of Line 1
FAIRTEN2	Fairlead tension of Line 2
FAIRTEN3	Fairlead tension of Line 3
ANCHTEN1	Anchor tension of Line 1
ANCHTEN2	Anchor tension of Line 2
ANCHTEN3	Anchor tension of Line 3

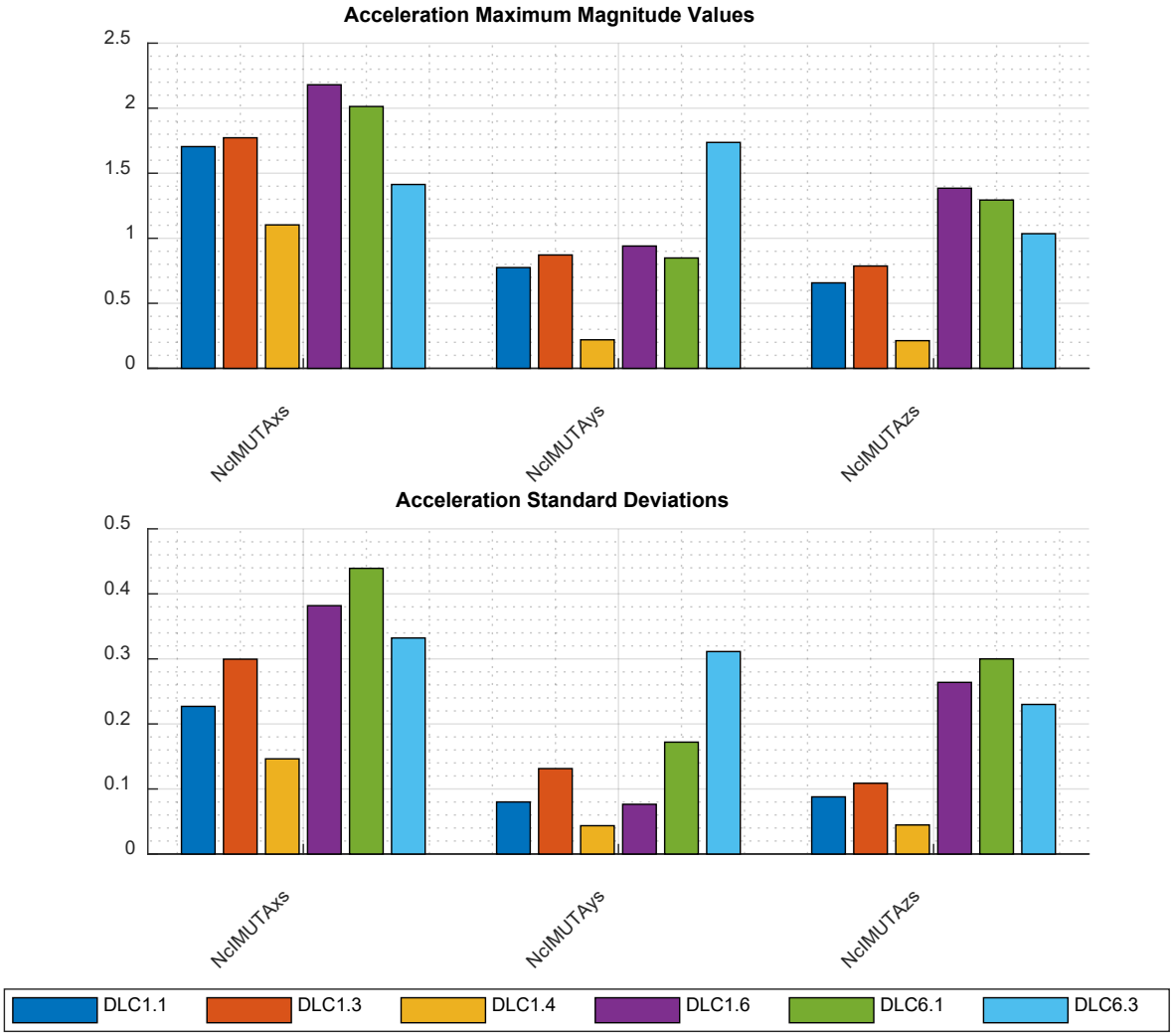

Figure 21. DLC acceleration statistics (m/s^2)

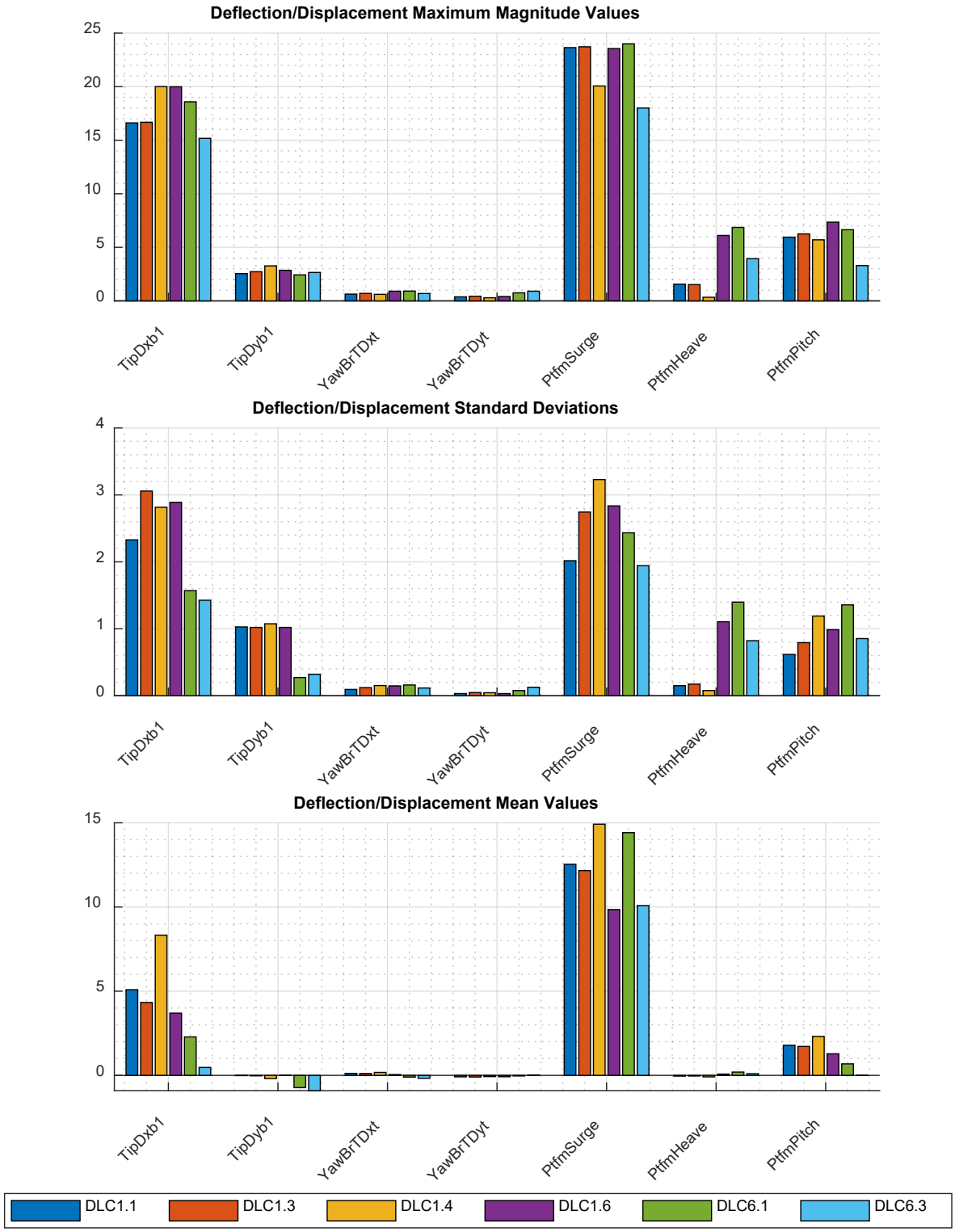

Figure 22. DLC deflection and displacement statistics (m or °)

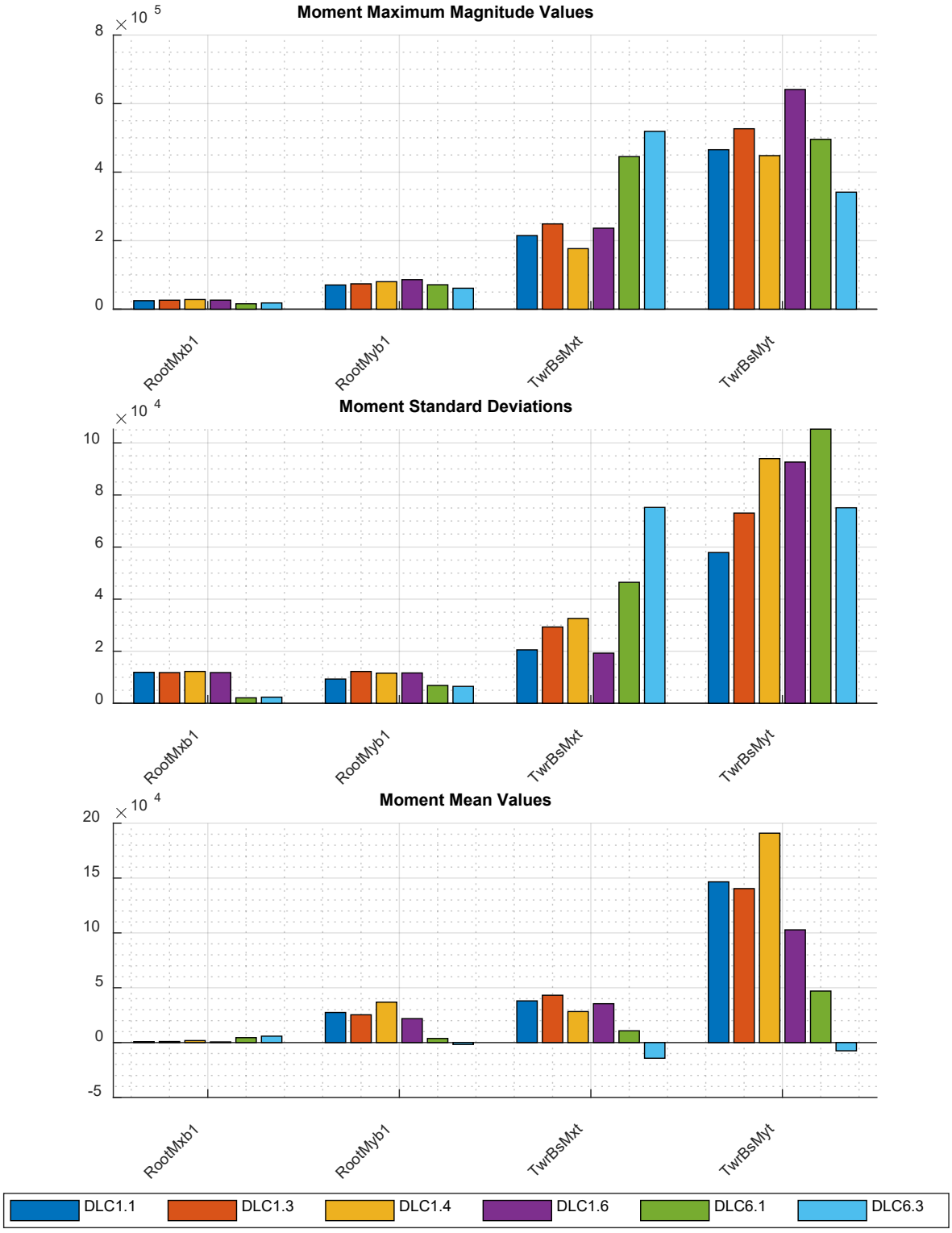

Figure 23. DLC moment statistics (kN-m)

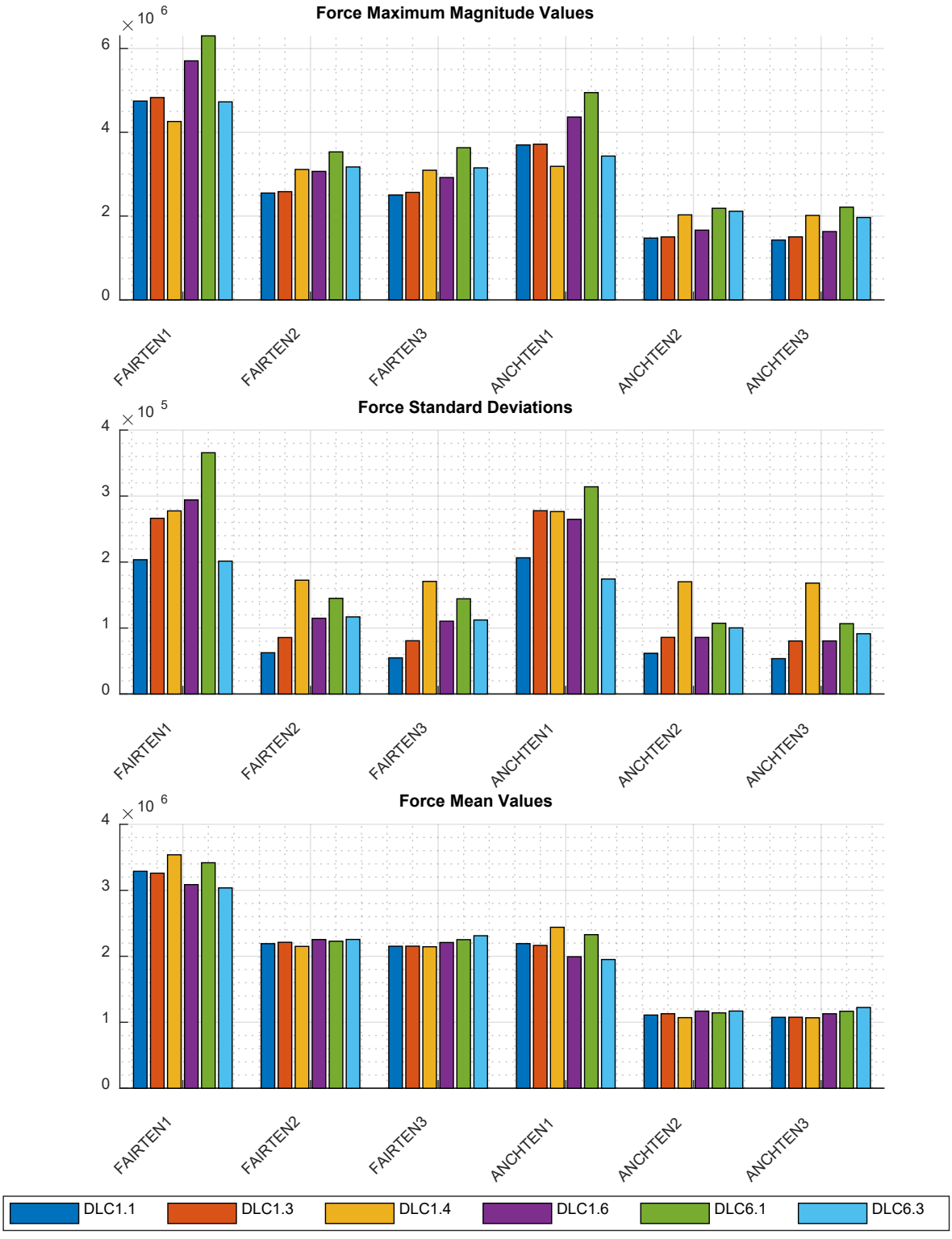

Figure 24. DLC force statistics (N)

References

Bir, G. 2005. *User's Guide to BModes* (Technical Report). Golden, CO: National Renewable Energy Laboratory. NREL/TP-500-39133. https://www.nrel.gov/docs/fy06osti/39133.pdf.

Chakrabarti, S. 2005. *Handbook of Offshore Engineering*. Oxford, UK: Elsevier Ltd.

Coulling, A. J., A. J. Goupee, A. N. Roberston, J. M. Jonkman, H. J. Dagher. 2013. "Validation of a FAST semi-submersible floating wind turbine numerical model with DeepCWind test data." *Journal of Renewable and Sustainable Energy*. https://aip.scitation.org/doi/10.1063/1.4796197.

Det Norske Veritas. 2010. Recommended Practice DNV-RP-C205. *Environmental Conditions and Environmental Loads*. https://rules.dnvgl.com/docs/pdf/dnv/codes/docs/2010-10/rp-c205.pdf.

DNV-GL. 2018 *Offshore Standards; DNVGL-OS-E301: Position Mooring*. http://rules.dnvgl.com/docs/pdf/dnvgl/os/2018-07/dnvgl-os-e301.pdf.

Duarte, T., A. Sarmento, M. Alves, J. Jonkman. 2013. "State-Space Realization of the Wave-Radiation Force within FAST." Presented at the ASME 2013 32nd International Conference on Ocean, Offshore and Artic Engineering, Nantes, France, June 9–14, 2013. Golden, CO: National Renewable Energy Laboratory. NREL/CP-5000-58099. https://www.nrel.gov/docs/fy13osti/58099.pdf.

Gaertner, E., J. Rinker, L. Sethuraman, F. Zahle, B. Anderson, G. Barter, N. Abbas, F. Meng, P. Bortolotti, W. Skrzypinski, G. Scott, R. Feil, H. Bredmose, K. Dykes, M. Shields, C. Allen, A. Viselli. 2020. *IEA Wind TCP Task 37: Definition of the IEA Wind 15-Megawatt Offshore Reference Wind Turbine* (Technical Report). Golden, CO: National Renewable Energy Laboratory. NREL/TP-5000-75698. https://www.nrel.gov/docs/fy20osti/75698.pdf.

Greenshields, C. J. 2011. "OpenFoam: Open Source CFD: Documentation." OpenFOAM Foundation Ltd. https://www.openfoam.com/documentation/. Accessed June 11, 2020.

Hall, M., and A. Goupee. 2015. "Validation of a lumped-mass mooring line model with DeepCwind semisubmersible test data." *Ocean Engineering,* Vol. 104, pp. 590-603. https://doi.org/10.1016/j.oceaneng.2015.05.035. https://www.sciencedirect.com/science/article/pii/S0029801815002279?via%3Dihub.

International Electrotechnical Commission (IEC). 2005. IEC 61400-1: Wind Tubines - Part 1: Design Requirements, 3rd Edition.

Jonkman, J. M., A. N. Robertson, and G. J. Hayman. Forthcoming. "HydroDyn User's Guide and Theory Manual." Golden, CO: National Renewable Energy Laboratory.

Lee, C. H. 1995. *WAMIT Theory Manual*. Massachusetts Institute of Technology, Department of Ocean Engineering, Cambridge, Massachusetts.

Musial, W., P. Beiter, P. Spitsen, J. Nunemaker, V. Gevorgian. *2018 Offshore Wind Technologies Market Report*. U.S. Department of Energy, Office of Scientific and Technical Information, Oak Ridge, TN. https://www.energy.gov/sites/prod/files/2019/09/f66/2018%20Offshore%20Wind%20Technologies%20Market%20Report.pdf.

National Renewable Energy Laboratory (NREL). 2020a. Wind Plant Integrated System Design and Engineering Model (WISDEM), https://github.com/WISDEM/WISDEM. Accessed June 11, 2020.

NREL. 2020b. Reference OpenSource Controller (ROSCO) for wind turbine applications, https://github.com/NREL/rosco. Accessed 6/11/2020.

Robertson, A., J. Jonkman, M. Masciola, A. Goupee, A. Coulling, C. Luan. 2014. *Definition of the Semisubmersible Floating System for Phase II of OC4* (Technical Report). Golden, CO: National Renewable Energy Laboratory. NREL/TP-5000-60601. https://www.nrel.gov/docs/fy14osti/60601.pdf.

Schwartz, Marc, Donna Heimiller, Steve Haymes, Walt Musial. 2010. Assessment of Offshore Wind Energy Resources for the United States (Technical Report). Golden, CO: National Renewable Energy Laboratory. NREL/TP-500-45889. https://www.nrel.gov/docs/fy10osti/45889.pdf.

Stewart, G. M., A. Roberston, J. Jonkman, M. A. Lackner. 2015. "The creation of a comprehensive metocean data set for offshore wind turbine simulations." *Wind Energy,* pp. 1151-1159. https://doi.org/10.1002/we.1881. https://onlinelibrary.wiley.com/doi/full/10.1002/we.1881.

Viselli, Anthony, H. J. Dagher, and Andrew Goupee. 2014. "Volturnus 1:8 – Design and testing of the first grid-connected offshore wind turbine in the U.S.A." in *19th Offshore Symposium Sponsored by the Texas Section of SNAME*, Houston, TX, 2014. https://www.onepetro.org/conference-paper/SNAME-TOS-2014-015?sort=&start=0&q=Design+and+testing+of+the+first+grid-connected+offshore+wind+turbine+in+the&from_year=&peer_reviewed=&published_between=&fromSearchResults=true&to_year=&rows=25#

Viselli, Anthony M., Andrew J. Goupee, and Habib J. Dagher. 2015a. "Model Test of a 1:8-Scale Floating Wind Turbine in the Gulf of Maine." *Offshore Mech. Arct. Eng*. 137(4): 041901. https://doi.org/10.1115/1.4030381.

Viselli, Anthony M., Andrew J. Goupee, Habib J. Dagher, and Christopher K. Allen. 2015b. "Design and model confirmation of the intermediate scale VolturnUS floating wind turbine subjected to its extreme design conditions offshore Maine." *Wind Energy*. Vol. 19, pp. 1161-1177. https://doi.org/10.1002/we.1886.

Viselli, A. G. Z. Forristall, B. R. Pearce and H. J. Dagher. 2015c. "Estimation of extreme wave and wind design parameters for offshore wind turbines in the Gulf of Maine using a POT method." *Ocean Engineering,* vol. 104, pp. 649-658. https://doi.org/10.1016/j.oceaneng.2015.04.086.